SHEAR FAILURE AND NUMERICAL PERFORMANCE EVALUATION OF RC BEAM MEMBERS MADE WITH HIGH-STRENGTH MATERIALS

(Translation from Proceedings of JSCE, No.697/V-54, February 2002)

Satoshi TSUCHIYA Tetsuya MISHIMA Koichi MAEKAWA

The shear capacity of RC beam and column members using self-compacting high-strength concrete and high-strength steel is investigated. It is found that increasing the concrete compressive strength scarcely affects shear capacity of the concrete above about 50 MPa, the size effect becomes more significant, and that careful consideration of concrete strength is required for effective use of high-strength steel as stirrups. The experimental results and the current design equation are compared, and FE analysis is carried out using a shear transfer constitutive model considering the fracture phase of high-strength concrete. It is verified that this analytical method can approximately evaluate the shear capacity and deformation of RC beams using high-strength materials.

Keywords: *RC beam/column, shear capacity, self-compacting high-strength concrete, high-strength reinforcing bars, FE analysis, design equation*

Satoshi Tsuchiya is a manager of COMS Engineering Corporation, Japan. He obtained his D. Eng. from the University of Tokyo in 2001. He has been trying to make high-grade nonlinear structural analysis fit for practical use. His research interests cover the seismic performance evaluation and numerical simulation of reinforced concrete structures.

Tetsuya Mishima is a manager of structural engineering section in the technical research institute, technology division of Maeda Corporation, Japan. He obtained his D. Eng. from the University of Tokyo in 1992. He has been involved in some civil structural research and development and design projects, especially experimental and analytical research of structural engineering.

Koichi Maekawa is a professor in the Department of Civil Engineering at the University of Tokyo, Japan. He earned his D. Eng. from the University of Tokyo in 1985. The structural mechanics and constitutive laws for reinforced concrete have been investigated as his academic major background. He joined the project for development of self-compacting concrete in 1985-1989. After innovation of its prototype, he has been engaged in the project for micro-structural development of cementitious materials and computational durability assessment.

1. INTRODUCTION

Self-compacting concrete can be generally expected to exhibit high strength and high durability as a result of its low water-to-powder ratio. Following the development of self-compacting concretes incorporating superplasticizers [1][2], efforts to develop more effective use of high-strength concrete have been made at the level of design practice. High-quality high-strength reinforcing bars with an adequate yield plateau and excellent extensibility are also in manufacture already and are available on the market [3]. The use of such high-strength materials can reduce the dead weight of structures and the amount of reinforcement required, while also lowering costs and bringing about new rational construction methods [4]. As infrastructure development in Japan gradually expands into areas of steep mountains and the deep underground space, the significance of effective practice for using high-strength properties including self-compactability is likely to grow more and more important.

Basic research is underway in an effort to identify the properties of RC members and structures that make use of high-strength materials, and the particular properties of such high strength materials are gradually becoming clear. Integrating this knowledge into a new technology for performance verification is greatly relevant at the present time ([3][6]-[9] and others). Previous studies have reported that, as the size of structures increases, the nominal shear strength of high-strength concrete decreases considerably as compared to that of normal-strength concrete (see [7][8] for example). Significant autogenous shrinkage has been pointed out as one possible reason for this decrease in strength [30].

With few examples of the application of high-strength materials, the design specifications define greater safety factors and upper limits for applicable strength ranges [10], but as technology advances these are expected to converge to suitable levels. In view of the fact that there has been little accumulation of knowledge about the properties of high-strength deformed reinforcing bars in the highly plastic range and the interaction between high-strength concrete and steel when these materials are combined, there is a need for much more research in this area. In this study, the authors will use existing numerical analysis techniques as a point of departure to study the process of shear failure in RC members using high-strength materials.

The phenomenon of shear failure of RC members and structures made of normal strength materials can be approximately predicted by numerical analysis to a certain degree [11]. On this basis, if the properties of high-strength materials can be formulated as appropriate constitutive models of suitable accuracy, the applicable range of this numerical approach can be expanded based on existing models [12]. Two examples can be given to demonstrate why merely changing the strength values in the existing constitutive models will not suffice to reflect the mechanical properties of high-strength materials. One is the smoothing of cracking phases and reduction of transferred stress along crack planes [13] due to splitting of the aggregate. The other is sudden stress release after cracking (tension softening). These two issues are key points in the numerical performance evaluation carried out here.

Four series of loading tests on RC members up to shear failure are reported, and the results are compared with the current design equation [14] and the size effect is also discussed. A method is proposed for expanding the existing constitutive models for normal strength RC [12] to include high-strength materials, and this is verified using two-dimensional finite element analysis. For the purposes of this study, high-strength concrete is defined as concrete of strength up to the point that coarse aggregate splits at the crack surface and its coarseness drops dramatically. As a general guide, this means a compressive strength of 60 MPa or greater. For convenience, deformed bars with a yield strength of 700 MPa or greater will be referred to as high-strength reinforcement. All high-strength concrete used in this study is self-compacting concrete [1].

2. LOADING TESTS ON SHEAR-PRONE RC BEAMS

Loading tests are performed on shear-prone RC beams made with high-strength materials. In this study, self-compacting high-strength concrete is used to implement the four series of tests shown in **Table 1**. The experimental results are listed in the following tables along with predicted values calculated with the current design equation [14] (to be covered later).

Table 1 Details and characteristics of each loading test

Series	No.	Size	Longitudinal Reinf.	Web Reinf.	Concrete	Steel	Purpose
1	9	Small	Main only 1/2 row	No	high/normal strength	high/normal strength	Verification of analytical method
2	2	Small	Main + Side (column)	No	high/normal strength	normal strength	Effect of side reinf.
3	3	Medium/ Large	Main only 2 row	Yes/No	High strength	normal strength	Size effect, web reinf. effect in large member
4	5	Small	Main only 1 row	Yes/No	high/normal strength	high strength	High-strength web and concrete strength relation

2.1 Test Series 1

In this series, loading tests are conducted on shear-prone small RC beam specimens without web reinforcement. The tests are distinguished by single and double row arrangements of main reinforcement, and by preparation of specimens with a combination of both normal and high-strength concrete and reinforcement. As shown in **Table 2** and **Fig. 1**, a total of nine specimens are prepared of standard size: beam height h = 300 mm, width b = 150 mm, and total member length L = 2,700 mm (except Specimen 9, whose length is L = 2,400 mm). Three experimental parameters are established: concrete strength (ordinary and high strength), reinforcement yield strength (ordinary and high strength), and arrangement method of main reinforcement (single and double row). The reinforcement arrangements are basically divided into two types: Specimens 1-4 and 9, in which two D19 reinforcing bars are placed in a single row, and Specimens 5-8, in which eight D10 reinforcing bars are placed in double row, as shown in **Fig. 1**. The dimensions are determined such that the reinforcement ratio is almost exactly equal. The shear span is set to 780 mm, and two-point concentrated bending/shear loading is conducted (with a pure bending span of 600 mm). Effective depths are slightly different for Specimens 1-4 and 9 and Specimens 5-8, and the shear span to depth ratios also differ. Specimen 9 is prepared for reference purposes, in order to investigate the anchoring behavior of the main reinforcement. As shown in Figure 1, the anchor length is made deliberately short.

Table 2 Summary of specimens and experimental results (Series 1)

	f'_c (MPa)	f_y (MPa)	Rebar D, No.	No. of Cracks[#]	V_{c_exp} (kN)	V_{c_cal} (kN)
No.1	69.5	711	D19, 2	5	47.8	54.4
No.2	29.4	711	D19, 2	6	38.9	46.6
No.3	69.5	333	D19, 2	5	46.8	54.4
No.4	29.4	333	D19, 2	5	46.5	46.6
No.5	69.5	1050	D10, 8	11	47.1	49.6
No.6	29.4	1050	D10, 8	6	49.4	42.6
No.7	69.5	363	D10, 8	10	45.9	49.6
No.8	29.4	363	D10, 8	6	46.6	42.6
No.9	69.5	711	D19, 2	7	43.7	54.4

f'_c: concrete compressive strength, f_y: steel yield strength, V_{c_exp}: diagonal cracking load (experiment), V_{c_cal}: diagonal cracking load (design eq.(1)), No. of Cracks[#]: number of cracks within a pure bending span

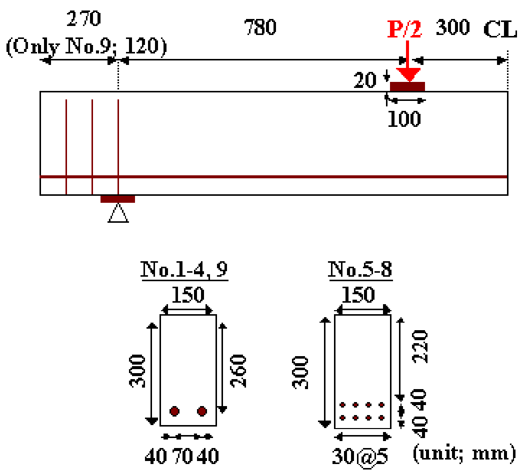

Fig. 1 Structural dimensions and loading method (Series 1)

Self-compacting high-strength concrete blended with fly ash is used. The concrete is cast vertically from the loading surface (in all four test series). However, with self-compacting concrete, it is thought that almost no segregation occurs whatever the casting direction. USD685 and USD785 are used for high-strength reinforcing bars D19 and D10, respectively, and SD345 is used for normal-strength reinforcing bars D19 and D10. Although USD685 has the same expansion properties as normal-strength deformed bars, no clear yield plateau is evident and the extensibility is slightly lower in the case of USD785 [3]. In this series of loading tests, however, the extensibility of the main reinforcement may not be an issue since shear failure occurs prior to yielding of the main reinforcement. With Specimens 5-8, the spacing between reinforcing bars is quite narrow, but since the concrete is self-compacting and resists segregation, it can be cast without problem. After wet curing, the specimens are subjected to loading at the age of 26 to 35 days. **Table 3** shows the concrete mixture used.

Table 3 Concrete mixture (Series 1)

Normal strength	G_{max} (mm)	slump (cm)	W/C (%)	air (%)	s/a (%)	Unit weight (kg/m^3)						
						W	C	S_1	S_2	G	AD	AE
	20	8	50	4.4	48.1	186	372	494	337	914	3.72	1.48
High strength	G_{max} (mm)	flow (cm)	W/C (%)	air (%)	V_w/V_p (%)	Unit weight (kg/m^3)						SP (P*%)
						W	C	FA	S_1	S_2	G	
	20	60	37.6	2.0	83.0	168	447	134	449	459	772	1.5

S_1: sea sand, S_2: crushed sand

Figs. 2-1 through **2-9** show the relationship between shear force and deflection at the bottom edge in the center of the beam. In the figures, V_c indicates the load value at which diagonal cracking first propagates, while V_{max} is the maximum shear force once the load-carrying capacity increases again. Specimens 1-4 and 9, with a single row of main reinforcement, fail immediately after diagonal cracking occurred. However, in the case of Specimens 5-8 with a double row of main reinforcement, the load-carrying capacity drops after diagonal cracking and is then restored again. In the case of Specimen 5, in particular, the load-carrying capacity rises to 163 kN and secondary and tertiary diagonal cracks with small inclination are induced, leading to ultimate failure. The two dense rows of thin reinforcing bars are thought to be the source of the high additional load-carrying capacity after diagonal cracking. Further, when high-strength concrete is used, the area in which diagonal cracking first progresses appears to be slightly closer to the loading points than in the case of ordinary concrete. This trend is difficult to recognize in the small specimens, but it is conspicuous in the loading tests conducted using the medium- and large-scale specimens in Series 3. **Fig. 3** shows the cracking situation after loading of typical Specimens 1 and 5. In the case of Specimen 5, diagonal cracking occurs near the loading points first, leading to a decrease in capacity, then the capacity increases again and secondary and tertiary diagonal cracking occur; this is discussed in detail in Section 5, where numerical analysis is carried out. In the case of the Specimen 9, whose anchor length is made intentionally short, the diagonal cracking load is about 10 % less than in the case of Specimen 1 with the same reinforcement arrangement and material; however, splitting failure due to insufficient anchor length does not occur.

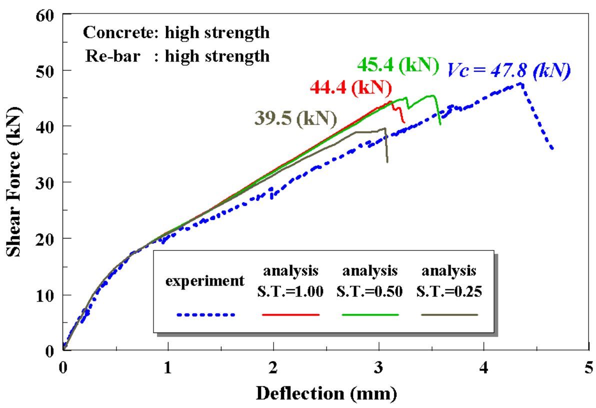

Fig. 2-1 No. 1 shear force – deflection relationship

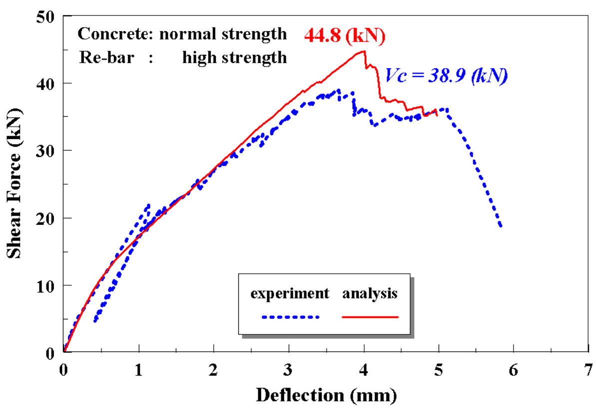

Fig. 2-2 No. 2 shear force – deflection relationship

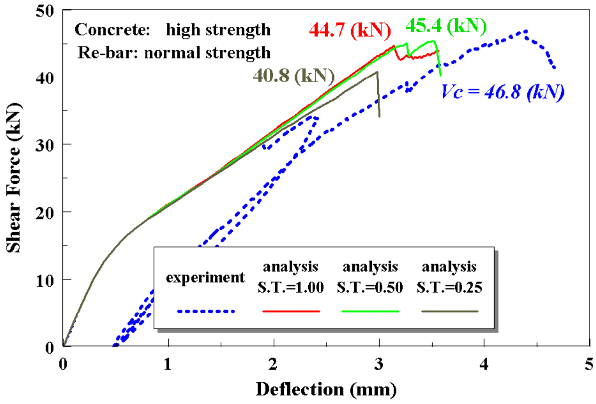

Fig. 2-3 No. 3 shear force – deflection relationship

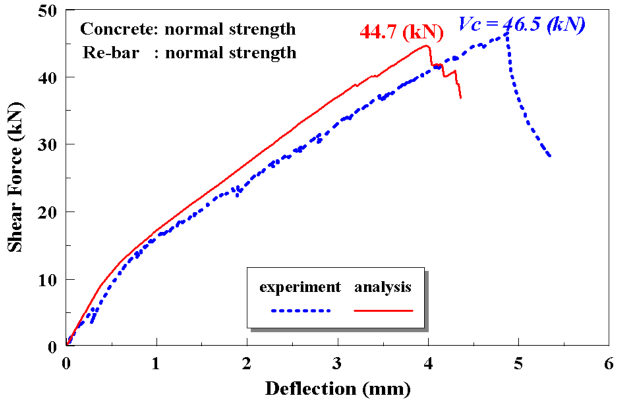

Fig. 2-4 No. 4 shear force – deflection relationship

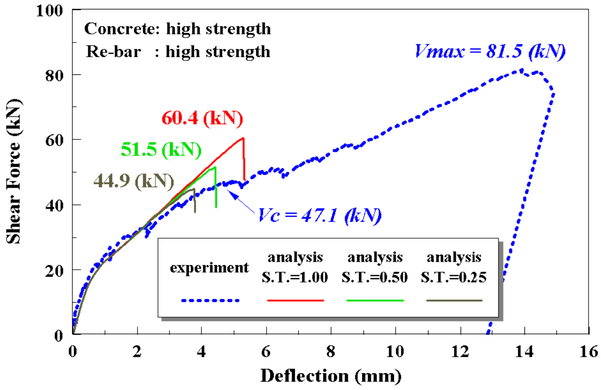

Fig. 2-5 No. 5 shear force – deflection relationship

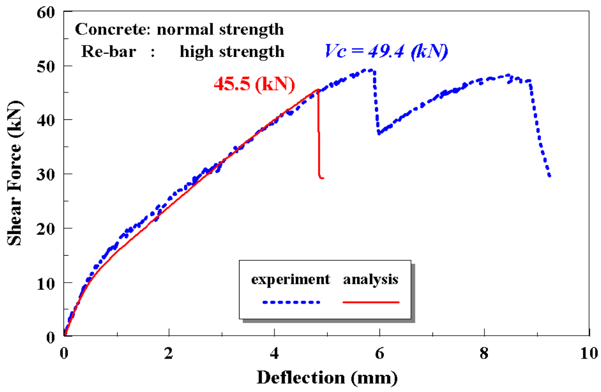

Fig. 2-6 No. 6 shear force – deflection relationship

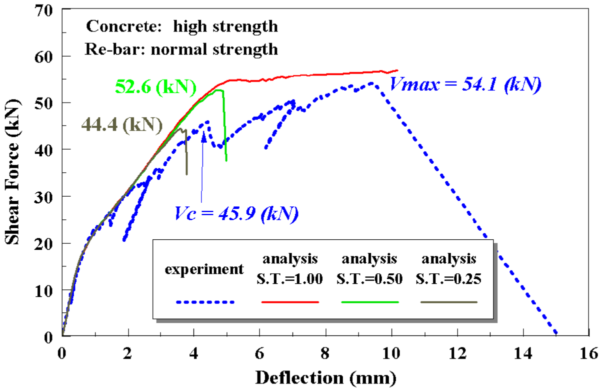

Fig. 2-7 No. 7 shear force – deflection relationship

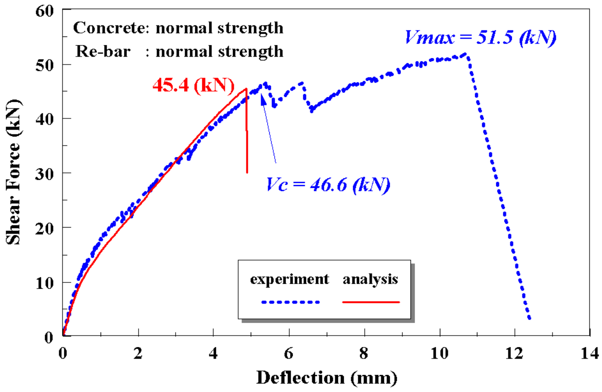

Fig. 2-8 No. 8 shear force – deflection relationship

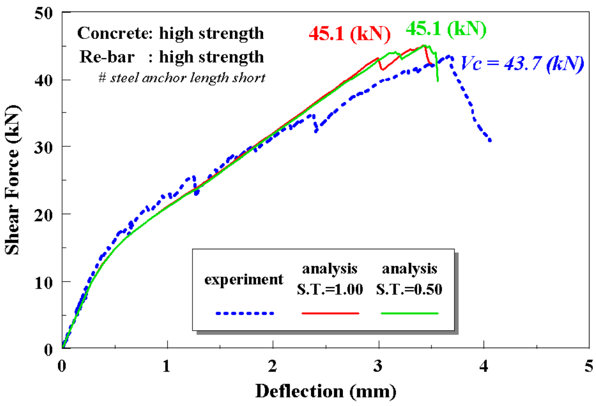

Fig. 2-9 No. 9 shear force – deflection relationship

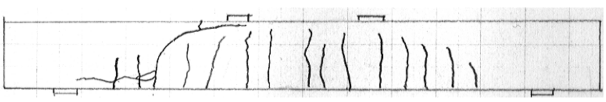

(a) Specimen 1

(b) Specimen 5

Fig. 3 Crack distribution

When high-strength concrete is used, both the initial stiffness and flexural cracking load are greater than with normal-strength concrete, yet the diagonal cracking load is almost the same regardless of concrete strength (**Fig. 2-1** to **Fig. 2-9**). This result is consistent with previous studies [3][6]–[9]. Main reinforcement strength does not affect the diagonal cracking load because shear failure precedes flexural yielding. The experimental results are summarized in **Table 2**.

2.2 Test Series 2

This study is carried out with RC beam and column members containing side reinforcement. Small specimen N250 using normal-strength concrete and specimen H250 using self-compacting high-strength concrete are picked up from a previous loading test that were implemented with the objective of studying the size effect [29]. For this reason, the water-to-cement ratio of the high-strength concrete is higher than in the other series. Although different experimental conditions, such as the stress derived from shrinkage, can be expected as a result, we proceed here with a macroscopic comparative study and ignore such differences. **Table 4** and **Fig. 4** show an outline of the specimens. Both measure h = 250 mm, b = 250 mm, d = 231 mm, and L = 2000 mm. Sectional dimensions are determined based on an actual railway viaduct, and the scale reduction is set at 5/16. For this reason, the cover concrete is relatively thin as compared to the small specimens generally used for tests, and small-diameter reinforcing bars are used in a dense arrangement similar to actual members. Although these specimens are designed to resemble column members, concentrated one-point loading is applied at the center and the shear span to depth ratio is set to 3.0.

Table 4 Specimen comparison and experimental results (Series 2)

	Rebar D, No.	f'_c (MPa)	f_y (MPa)	V_{c_exp} (kN)	V_{c_cal} (kN)
H250	D10, 20	58.7	346	86.6	87.6
N250	D10, 20	29.7	346	63.7	75.4

f'_c: concrete compressive strength, f_y: steel yield strength, V_{c_exp}: diagonal cracking load (experiment), V_{c_cal}: diagonal cracking load (design eq.(1))

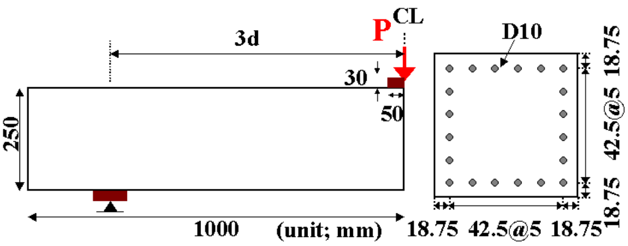

Fig. 4 Structural dimensions and loading method (Series 2)

The concrete is blended with fine limestone powder with the objective of ensuring self-compactability, and SD295 (twenty D10 deformed bars) is used for all of the specimens. Since the intention is to unify the sectional size ratio for different scales of specimens, the spacing between reinforcing bars is small. This might lead to some concern regarding concrete compaction and segregation, but in fact the problems do not materialize. After wet curing, loading is carried out at the age of 14 days in the case of H250 and 30 days in the case of N250. **Table 5** shows the concrete mixture used here.

Table 5 Concrete mixture (Series 2)

Normal strength	G_{max} (mm)	slump (cm)	W/C (%)	air (%)	s/a (%)	Unit weight (kg/m^3)							
						W	C	S_1	S_2	G_s	G_l	AE	
	20	8	58.9	4.0	44.6	162	275	490	326	477	583	2.75	
High strength	G_{max} (mm)	flow (cm)	W/C (%)	air (%)	V_w/V_p (%)	Unit weight (kg/m^3)						SP (P*%)	WG (W*%)
						W	C	LS	S	G_s	G_l		
	20	60	46.0	2.0	80.0	184	400	270	712	352	430	1.8	0.1

S_1: land sand, S_2: crushed sand, G_s: aggregate 5-13mm, G_l: aggregate 13-20mm, WG: segregation-reduction agent

Figs. 5-1 and **5-2** show the relationship between shear force and deflection at the bottom edge in the center of the beam. Diagonal cracks propagate almost simultaneously with yielding of the main reinforcement in the case of H250 and before yielding in the case of N250. In both cases, failure occurs immediately after diagonal cracking. No splitting cracks occur along the main reinforcement.

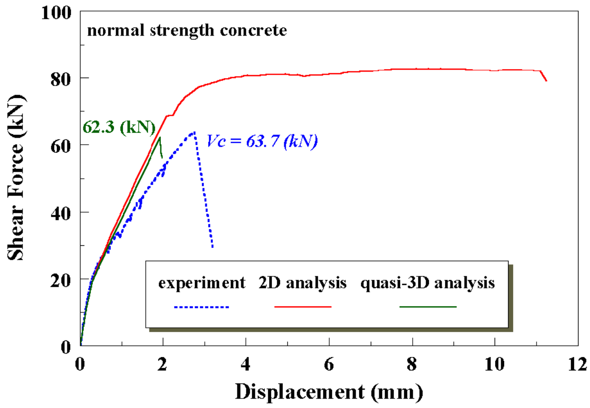

Fig. 5-1 N250 shear force – deflection relationship

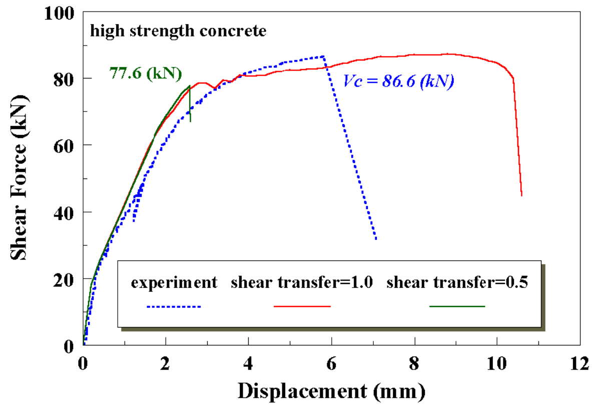

Fig. 5-2 H250 shear force – deflection relationship

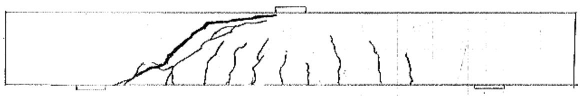

Fig. 6-1 N250 crack distribution

Fig. 6-2 H250 crack distribution

A look at the cracking pattern shows that in both specimens there is a distribution of cracks, even in the case of diagonal cracks. It is thought that this is caused by the bonding effect of the side reinforcement. As concrete strength increases, the diagonal cracking load increases as well, and the cracking tendency differs qualitatively from that in the Series 1 loading tests (**Figs. 5-1** and **5-2**). In previous tests [15][16] with normal-strength concrete, it was reported that shear capacity may be increased by adding side reinforcement. Although detailed study will be necessary in future with more samples to look into the effects of specimen size and material properties, it does appear from these results that side reinforcement is effective at distributing the diagonal cracks and increasing the shear capacity of RC beams made with high-strength materials. **Figs. 6-1** and **6-2** show the post-loading damage, while **Table 4** gives a summary of the experimental results.

2.3 Test Series 3

The Series 3 loading tests are conducted on shear-prone RC beam specimens of both medium and large sizes. The objective is to study the reduction in nominal concrete shear strength accompanying greater structural size and also the shear failure characteristics using an RC beam with web reinforcement. (In other words, the aim is to study the size effect.) **Table 6** and **Fig. 7** show an outline of the specimens. Three specimens are studied in all: Specimen 1 of medium size (h = 890 mm, b = 400 mm, d = 800 mm, and L = 7,200 mm), and larger Specimens 2 and 3 (h = 1,300 mm, b = 500 mm, d = 1,200 mm, and L = 10,000 mm). Large specimen 3 is provided with web reinforcement. Regarding the structural dimensions of the large specimens, the effective depth is made as large as possible within the limitations of the available loading facilities and transport jigs. Furthermore, details of the reinforcement arrangement are designed so that the main reinforcement ratio is almost equal in each case. The shear span for each specimen is determined such that the shear span to depth ratio is 3.0, and concentrated two-point bending/shear loading is applied. The pure bending moment span is set to 800 mm for all specimens.

Self-compacting high-strength ready-mixed concrete containing silica fume is used; the mixture is shown in **Table 7**. For reinforcing bars, normal strength SD295 or SD345 are used. After wet curing, loading is applied at the age of 26 to 28 days after casting.

Figs. 8-1 through **8-3** show the relationship between shear force and deflection at the bottom edge in the center of the beam. In these figures, V_y indicates shear force at the point where the load-carrying capacity of the beam with web reinforcement decreases during loading. In the case of Specimen 1, load-carrying capacity decreases simultaneously with the initiation of diagonal cracking. In the case of Specimen 2, load-carrying capacity increases slightly after the initiation of diagonal cracking, and then, secondary diagonal cracking occurs in another shear span at the symmetric side, leading to failure. In both of these specimens, as in the Series 1 loading tests, the first diagonal cracks propagate toward the loading points on the shear span. It is thought that the use of medium and large-size specimens makes this tendency more conspicuous. In the case of Specimen 3, which includes web reinforcement, after initial diagonal cracking at an approximately 45-degree angle, load-carrying capacity continues to increase until the progression of secondary and tertiary diagonal cracking at approximately 30 degrees. Ultimately, shear displacement along the tertiary diagonal cracks is accompanied by a drop in load-carrying capacity and almost simultaneous yielding of the main reinforcement.

Table 6 Summary of specimens and experimental results (Series 3)

	No.1	No.2	No.3
b*h*L (mm)	400*890 *7200	500*1300 *10000	500*1300 *10000
d (mm)	800	1200	1200
f'_c (MPa)	72.7	77.6	82.5
Main Rebar D, No.	D13*2;C D25*10;T	D19*2;C D35*2;T	D19*2;C D35*2;T
f_y (MPa)	338.6;C 393.9;T	387.9;C 382.4;T	387.9;C 382.4;T
f_{wy} (MPa)	-----	-----	338.6
p_w	0%	0%	0.169% (D13@300)
V_{c_exp} (kN)	307.0	467.4	498.4
V_{c_cal} (kN)	345.5	586.7	586.7
V_{s_exp} (kN)	-----	-----	605.8
V_{s_cal} (kN)	-----	-----	298.4

f_{wy}: stirrup yield strength, p_w: web reinforcement ratio, V_{c_exp}: diagonal cracking load (experiment), V_{c_cal}: diagonal cracking load (design eq.(1)), V_{s_exp}: truss load (experiment), V_{s_cal}: truss load (design eq.(2))

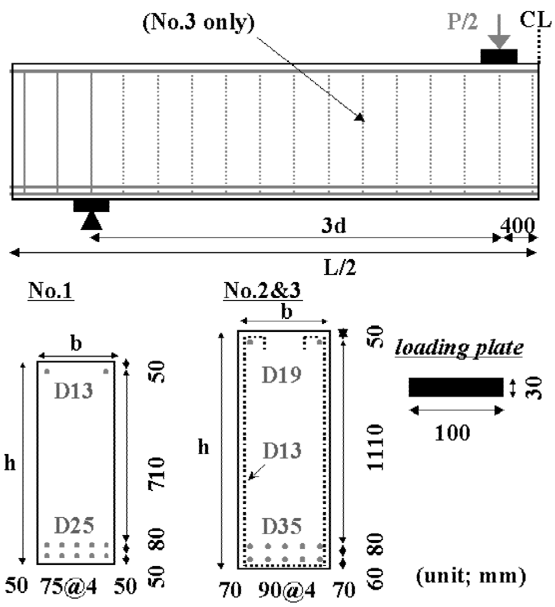

Fig. 7 Structural dimensions and loading method (Series 3)

Table 7 Concrete mixture (Series 3)

G_{max} (mm)	flow (mm)	W/C (%)	air (%)	V_w/V_p (%)	Unit weight (kg/m³)						SP (P*%)
					W	C	SF	S_1	S_2	G	
20	600	35.0	2.0	106	165	424	47	666	230	843	1.4

S_1: land sand, S_2: crushed sand

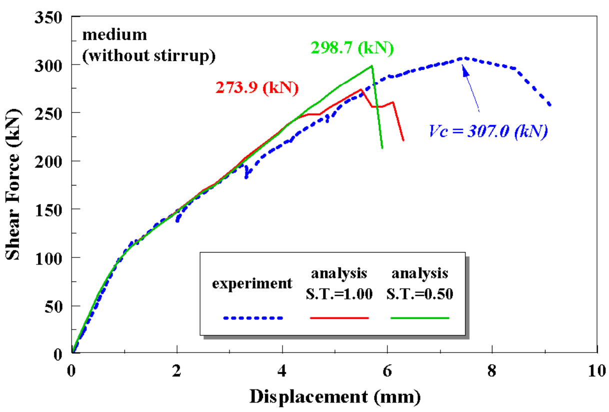

Fig. 8-1 No.1 shear force – deflection relationship

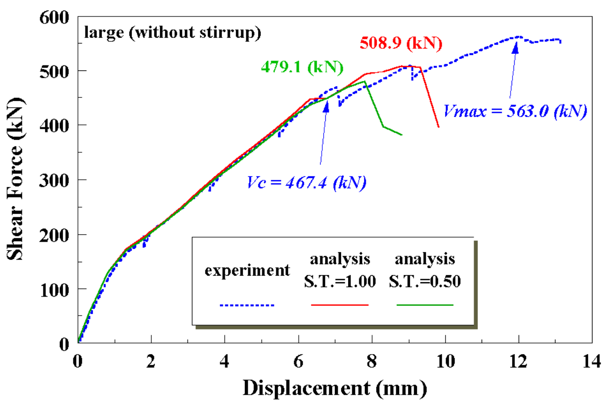

Fig. 8-2 No.2 shear force – deflection relationship

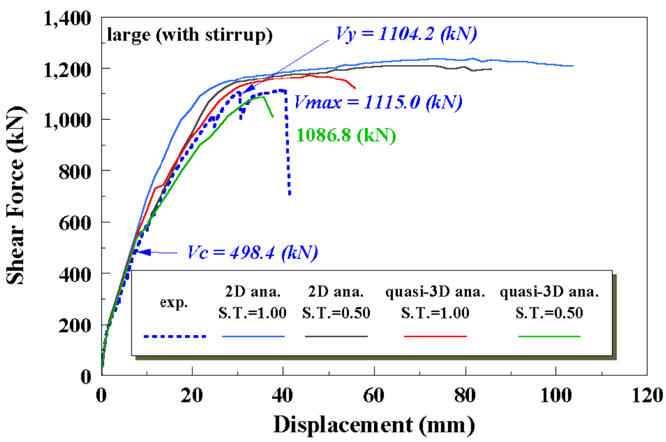

Fig. 8-3 No.3 shear force – deflection relationship

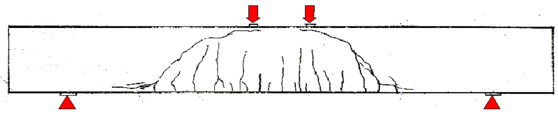

Fig. 9-1 Specimen 1 crack distribution

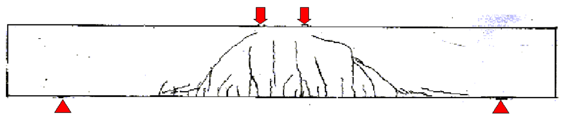

Fig. 9-2 Specimen 2 crack distribution

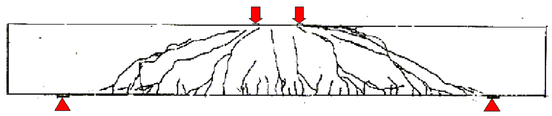

Fig. 9-3 Specimen 3 crack distribution

A look at the flexural cracking pattern shows that the crack distribution is limited to the vicinity of the main reinforcement in tension, and that the cracks become discrete wherever they diverge from the reinforcement. This is the same tendency as seen in loading tests [17] with large RC beams made of normal-strength concrete. **Figs. 9-1** through **9-3** show the damage condition after loading, while **Table 6** gives an outline of the experimental results.

2.4 Test Series 4

Loading tests [33] are conducted on shear-prone small RC beam specimens constructed with high-strength materials for both the concrete and the main and web reinforcement. The primary focus of the tests is the reinforcing effect of using high-strength reinforcing bars as web reinforcement, with the issue being the influence of concrete strength on the effectiveness of such reinforcement. In the Design Edition of the JSCE Standard Specification for Design and Construction of Concrete Structures [10], when high-strength reinforcing steel is used as web reinforcement, an upper limit for yield strength is prescribed for use in the design calculations (400 MPa). However, if self-compacting high-strength concrete is used, there is expectation that this upper limit may be revised upward. **Table 8** and **Fig. 10** give an outline of the test specimens. The dimensions are standardized at h = 400 mm, b = 400 mm, d = 350 mm, and L = 4000 mm.

Table 8 Summary of specimens and experimental results (Series 4)

	No.1	No.2	No.3	No.4	No.5
f'_c (Mpa)	51.0	49.4	55.2	27.8	51.0
Rebar D, No.	D10*2;C D29*4;T	D10*2;C D29*4;T	D10*2;C D29*4;T	D10*2;C D29*4;T	D10*2;C D29*4;T
f_y (Mpa)	803.0;C 698.2;T	803.0;C 698.2;T	803.0;C 698.2;T	803.0;C 698.2;T	803.0;C 698.2;T
f_{wy} (Mpa)	-----	746.6	746.6	746.6	803.0
p_w	-----	0.158% D6@100	0.211% D6@75	0.158% D6@100	0.178% D10@200
V_{c_exp} (kN)	194.7	178.9	186.2	144.6	169.1
V_{c_cal} (kN)	195.2	195.2	195.2	164.3	195.2
V_{s_exp} (kN)	-----	202.1	251.2	129.9	207.7
V_{s_cal} (kN)	-----	143.9	191.9	143.9	174.3

V_{c_exp}: diagonal cracking load (exp.), V_{c_cal}: diagonal cracking load (design eq.(1)), V_{s_exp}: truss load (exp.), V_{s_cal}: truss load (design eq.(2))

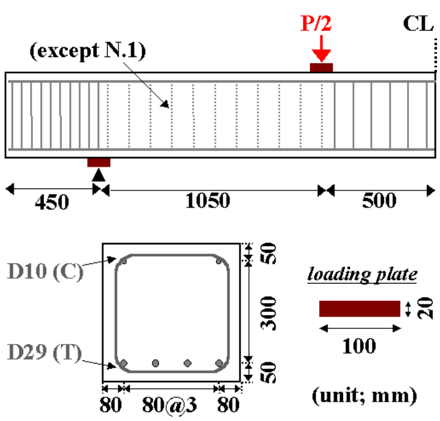

Fig. 10 Structural dimensions and loading method (Series 4)

Two experimental parameters are used: concrete strength (ordinary and high) and web reinforcement ratio. The shear span is fixed at 1,050 mm so that the shear span to depth ratio is 3.0, and two-point bending/shear loading is conducted. The pure bending moment span is set to 1,000 mm.

Self-compacting high-strength concrete formulated with low-heat cement is used. The water-to-cement ratio is set at 33 % and the attained strength at a material age of 28 days is estimated at 72.0 MPa. However, because there is little data in the region of around 50.0 MPa with shear failure, it is decided to apply loading at a younger material age. USD685 or SHD685 are used for the high-strength reinforcement. Both USD685 and SHD685 exhibit the similar expansive properties as normal-strength deformed reinforcements [3]. After wet curing, loading is conducted at a material age of approximately 14 days. **Table 9** shows the concrete mixture used.

Table 9 Concrete mixture (Series 4)

Normal strength	G_{max} (mm)	slump (cm)	W/C (%)	air (%)	s/a (%)	Unit weight (kg/m^3)				AD (C*%)	
						W	C	S	G		
	20	12	60.5	4.0	47.1	168	278	862	982	2.8	
High strength	G_{max} (mm)	flow (cm)	W/C (%)	air (%)	V_w/V_p (%)	Unit weight (kg/m^3)				SP (P*%)	AD (C*%)
						W	C	S	G		
	20	60	33.0	5.5	94.0	165	500	846	801	1.6	1.5

Figs. 11-1 through **11-5** show the relationship between shear force and deflection at the bottom edge in the center of the beam. For each of the specimens, shear failure occurs before flexural yielding. With the Specimen 1, which has no web reinforcement, capacity decreases with the occurrence of diagonal cracking. However, in the case of other specimens, which have web reinforcement, load-carrying capacity continues to increase even after the occurrence of diagonal cracking, and diagonal cracks with small inclinations are gradually induced. Ultimately, shear displacement progresses along the inclined crack surface, leading to a decrease in capacity.

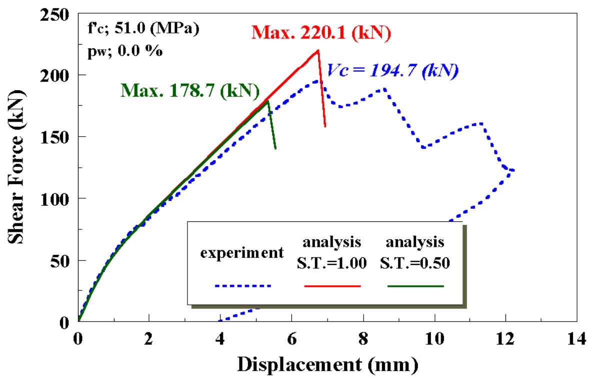

Fig. 11-1 No.1 shear force – deflection relationship

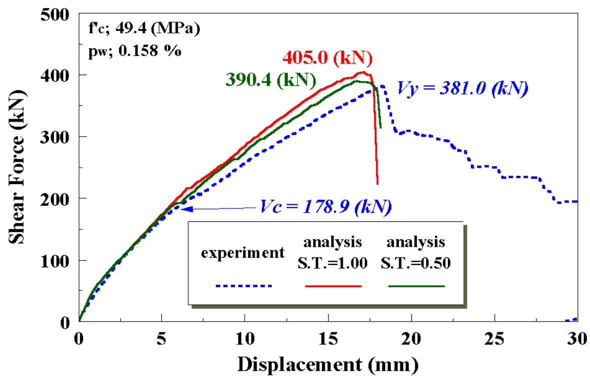

Fig. 11-2 No.2 shear force – deflection relationship

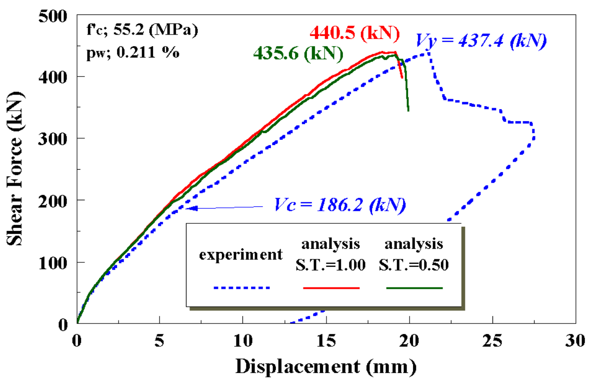

Fig. 11-3 No.3 shear force – deflection relationship

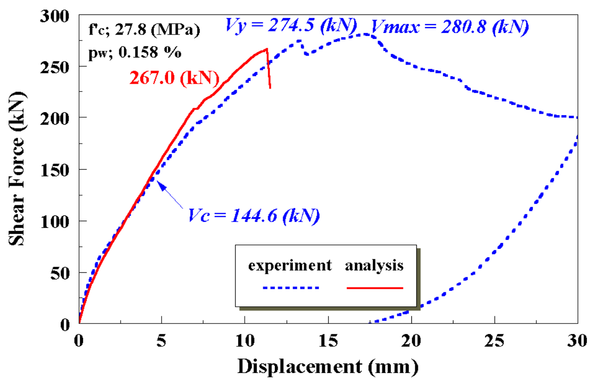

Fig. 11-4 No.4 shear force – deflection relationship

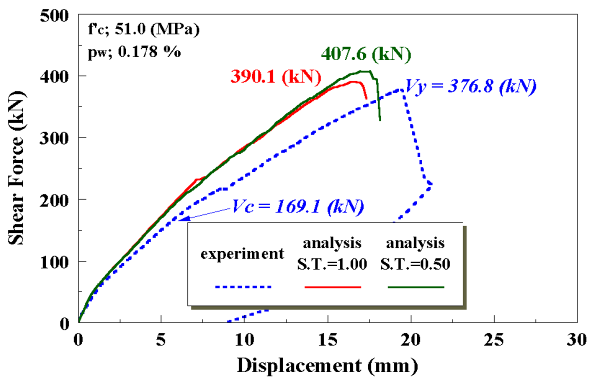

Fig. 11-5 No.5 shear force – deflection relationship

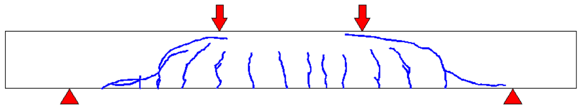

Fig. 12-1 Specimen 1 crack distribution

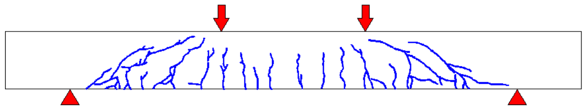

Fig. 12-2 Specimen 2 crack distribution

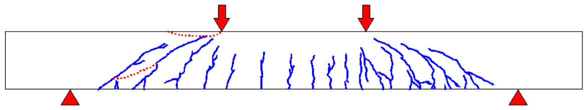

Fig. 12-3 Specimen 3 crack distribution

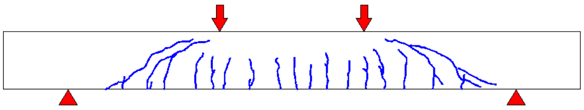

Fig. 12-4 Specimen 4 crack distribution

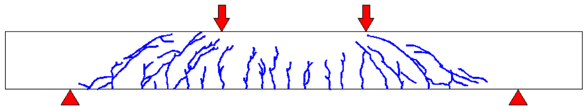

Fig. 12-5 Specimen 5 crack distribution

With specimens using high-strength concrete, capacity increases as the amount of web reinforcement is increased. However, the capacity seems to increase more effectively in the case of specimens with a distributed arrangement of small-diameter reinforcing bars. Although some variations are evident through visual observation, there is no obvious or clear correlation between diagonal cracking load and concrete strength. **Figs. 12-1** through **12-5** show the cracking pattern after loading, while **Table 8** gives a summary of the experimental results.

3. COMPARISON WITH CURRENT DESIGN EQUATION AND SIZE EFFECT

In this section, the experimental results described in the previous section are used in a comparative study with the current design equation as a means of examining the shear capacity of RC beams constructed with high-strength materials. In general, shear capacity is expressed as the sum of the shear capacity V_c contributed by the concrete (when diagonal cracking occurs) and the shear capacity V_s contributed by the web reinforcement. Truss theory is used to calculate V_s. The experimental results described in the section above will be categorized according to whether or not the specimens include web reinforcement, and the comparative study will be performed individually for V_c and V_s.

3.1 Concrete shear capacity Vc and size effect

The Niwa equation [14] is used for the diagonal cracking load. Here, the predicted value calculated using the design equation is expressed as $V_{c\text{-}cal}$. The Niwa equation is the basis of the shear capacity equation in the JSCE Standard Specification for Design and Construction of Concrete Structures [10], and it has been confirmed as highly accurate with regard to normal-strength materials and concentrated loading. This Standard Specification sets an upper limit on the compressive strength term with regard to the use of high-strength concrete, and the limit is applied as recommended in calculating V_{c_cal} in this paper. In other words, when the strength exceeds a prescribed value, the calculated value of diagonal cracking load does not rise further. The design equation is as shown below; and the safety factors are set at 1.0.

$$V_c / bd = 0.2 \cdot \sqrt[3]{f_c'} \cdot \sqrt[3]{100p} \cdot \sqrt[4]{1000/d} \cdot \left(0.75 + \frac{1.4}{a/d}\right), \quad \sqrt[3]{f_c'} \le 3.6 \tag{1}$$

where, V_c is diagonal cracking load (kN), f_c' is compressive strength as obtained with a cylinder test piece (N/mm^2), p is main tensile reinforcement ratio, b is member width (mm), d is effective depth (mm), and a is shear span (mm).

Even when there is no web reinforcement, the load is seen to increase slightly after the occurrence of diagonal cracking in some cases. Here, however, in accordance with the definition, the diagonal cracking load is treated as the limit state. The Niwa equation was originally a design equation used to calculate ultimate shear strength, and is not specifically for calculating diagonal cracking load. However, in the experiments described in this paper, the diagonal cracking point is taken to be the limit state from the following reasons; many of specimens have peculiar reinforcement arrangement, which is difficult to use in practice, so that flexural capacity would exceed shear capacity in spite of small size. It would be also understandable if diagonal cracking load is used in order separate V_c and V_s in the experiment.

In the Series 1 loading tests, where normal-strength concrete was used, the diagonal cracking capacity value (expressed as V_{c_exp}) is close to or greater than the value calculated by the design equation (V_{c_cal}), with the exception of Specimen 2 (**Table 2**). For specimens where high-strength concrete was used, V_{c_exp} is somewhat smaller than given by the design equation in all cases, with a value of approximately 86 %-95 % of V_{c_cal}. The diagonal cracking load reaches a maximum as strength increases. The results for the Series 1 loading tests confirm the validity of the current design equation with regard to the increase in concrete compressive strength.

For Specimen N250 in the Series 2 loading tests, in which concrete of normal strength was combined with side reinforcement, V_{c_exp} is approximately 85 % of V_{c_cal}. In contrast, for Specimen H250 in which high-strength concrete was used, V_{c_exp} and V_{c_cal} are almost the same (**Table 4**). Since the sectional size ratio of these specimens is almost identical to that of an actual bridge pier, the specimens have thinner cover concrete than is typical of laboratory specimens and there is a dense arrangement of reinforcement in the section. Despite this, the comparison with the current design equation reveals no major problems with accuracy. In calculating V_{c_cal}, the sectional neutral axis position is taken into account and fourteen reinforcing bars are placed in the tension zone of the section.

In the Series 3 loading tests with medium- and large-size RC beams, V_{c_exp} is lower than the value calculate with the design equation for all specimens, at approximately 80 %-85 % of V_{c_cal} (**Table 6**). This is the same trend as seen in the Series 1 loading tests. However, it is important to note that, as structural size increases, the size of the discrepancy increases somewhat as well. If the influence of the main reinforcement ratio and ratio of shear span to depth are as shown by Eq. (1), this would mean that the size effect is greater than in the case of normal-strength concrete. For Specimen 3 with web reinforcement, the diagonal cracking load has to be determined by visual observation.

In the Series 4 loading tests, the occurrence of diagonal cracking has to be confirmed visually for all except Specimen 1. For all specimens, V_{c_exp} is lower than V_{c_cal}, with a value about 88 % of the design equation value when normal-strength concrete is used and about 87 %-100 % when-high strength concrete is used (**Table 8**). Capacity is slightly lower when ordinary concrete is used, but apart from this, the trends are the same as for the Series 1, 2, and 3 tests.

From the results of these four series of loading tests, the nominal concrete shear strength is calculated and the relationship with effective depth, which is representative of structural size, is shown on a logarithmic scale in **Fig. 13**. Here, shear capacity is assumed to be proportional to the one-third power of main tensile reinforcement ratio, and all reinforcement ratios for the beam are converted to 1.59 % for display on the graph. The geometry, including the arrangement of reinforcing bars, is not uniform, and the amount of data is limited, so no definite conclusions can be drawn from this data. However, in broad terms, a reasonably good correlation can be seen between effective depth and shear capacity. Considering the variations in concrete compressive strength among the four test series, the effect of concrete strength on shear capacity can be indirectly regarded as not being very great. **Fig. 14** shows the relationship between the ratio of V_{c_exp} to V_{c_cal} and effective depth. In Eq. (1), the ratio of these two values would be greater if there were no upper limit established in the term for offsetting strength.

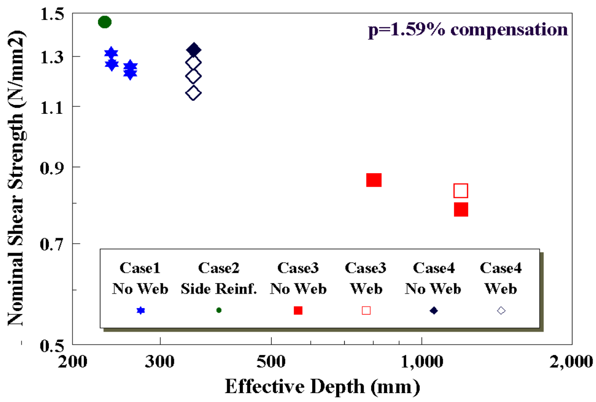

Fig. 13 Relationship between nominal shear strength – effective depth

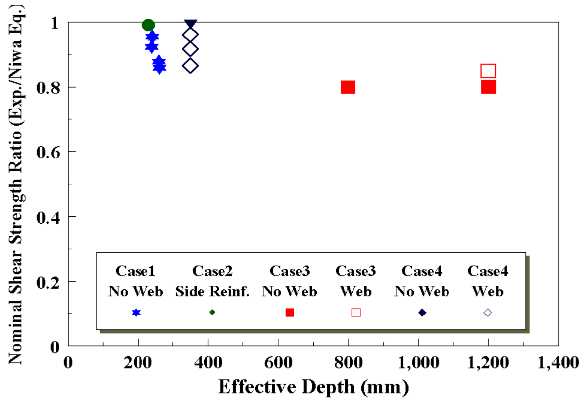

Fig. 14 Relationship between experiment/calculated value – effective depth relationship

3.2 Web reinforcement shear capacity Vs and Truss Theory

According to Truss Theory, Vs can be calculated using Eq. (2).

$$\begin{aligned} V_s &= A_w f_{wy}\left(\frac{\sin\alpha}{\tan\theta}+\cos\alpha\right)z/s \\ &= A_w f_{wy}\left(\frac{\sin\alpha}{\tan\theta}+\cos\alpha\right)d/1.15s \end{aligned} \tag{2}$$

where, V_s is the capacity contributed by truss action (kN), A_w is the total sectional area of one set of web reinforcement (mm^2), f_{wy} is the yield strength of the web reinforcement (N/mm^2), α is the angle formed by web reinforcement and the member axis, θ is the angle formed by the compressive arch and the member axis (assumed to be 45 degrees in design), z is the distance between centers of tension and compression (mm), d is effective depth (mm), and s is the spacing between web reinforcement (mm). In the Design Edition of the Standard Specification for Design and Construction of Concrete Structures published by the JSCE in 1996 [10], 400 MPa is established as the upper limit for f_{wy}.

It is known that with the modified Truss Theory the web reinforcement is generally evaluated on the safe side when its quantity is small [18]. Even after yielding of the web reinforcement, there is thought to be a mechanism by which the angle θ of the compressive arch decreases, thus increasing shear capacity [19]. In RC beams using normal-strength concrete, this limit is thought to be approximately tanθ = 0.5. However, up to now, no equations have been established that are capable of quantitatively evaluating the rise in capacity after yielding of the web reinforcement. Accordingly, in actual design, the capacity is evaluated on the safe side as θ = 45 degrees.

With Specimen 3 in the Series 3 loading tests, which contained normal-strength web reinforcement, V_{s_exp} is 605.8 kN. In contrast, the V_{s_cal} value calculated on the assumption of a 45-degree diagonal arch is 298.4 kN, a discrepancy of 2.03 times (**Table 6**). However, if tanθ = 0.5, V_{s_cal} becomes 596.9 kN, which brings it to almost the same value as V_{s_exp}. The value tanθ= 0.5 almost perfectly matches the angle of the diagonal cracks observed in the experiment. This can be interpreted as meaning that, after yielding of the web reinforcement, the compressive arch flattens out. Even when high-strength concrete (whose cracked surface is smoother) is used, the mechanism by which the web reinforcement resists external force after diagonal cracking is thought to be the almost same as when ordinary concrete is used.

For the Series 4 loading tests, in which high-strength reinforcing bars were used as web reinforcement, **Table 8** shows the values of V_{s_exp} and V_{s_cal}, which is calculated based on the actual yield strength of the web reinforcement. With Specimens 2, 3, and 5, which contain high-strength concrete, the ratio of V_{s_exp} to V_{s_cal} is from 1.19 to 1.40 as in the Series 3 loading tests, with the experimental values higher than the calculated values [9]. With Specimen 4, which contains normal-strength concrete, however, the value is 0.90, with the experimental value lower than the calculated value. Thus, when high-strength reinforcement is used as web reinforcement, the reinforcing effect differs greatly depending on the concrete strength. This result suggests that it would be possible to achieve a reinforcing effect comparable to the yield strength of high-strength reinforcement if careful consideration is given to an appropriate combination with concrete strength. Regarding the existing prescription for an upper limit to design yield strength of the web reinforcement at 400 MPa, the conclusion from this work is that there is room for further study.

A summary of the above discussion is presented in **Table 10**.

Table 10 Summary of RC beam experiment using high-strength concrete

Series 1	(1) Diagonal cracking load of RC beam is almost the same regardless of concrete strength. (2) Strength of main reinforcement does not affect deformation behavior. (3) In the case of specimens with double row arrangement of main reinforcement, the load-carrying capacity dropped after diagonal cracking and was then restored again.
Series 2	As concrete strength increases, diagonal cracking load also increases. (Although detailed study is necessary, such to investigate the effect of shrinkage, this might suggest the possibility of optimized design as a complex material.)
Series 3	(1) Size effect in nominal shear strength may be significant in large specimens. (2) First diagonal cracking area is toward the loading points on the shear span. (3) Sufficient reinforcing effect to shear can be obtained by normal strength web reinforcement.
Series 4	(1) Diagonal cracking load of RC beam is insensitive to concrete strength. (2) Full reinforcing effect equivalent to yield strength of high-strength web reinforcement can be obtained. (In the case of normal-strength concrete, full reinforcing effect equivalent to yield strength of high-strength web reinforcement can not be obtained.

4. SUMMARY OF NONLINEAR ANALYSIS METHOD

In this section, the behavior of members constructed with high-strength materials is analyzed theoretically with the aim of generalizing the factual record presented in the previous section. In addition, another strand of the study will deal with the applicability of numerical performance evaluation techniques to RC members.

4.1 Basic in-plane models

The two-dimensional nonlinear analytical method adopted in this study utilizes path-dependent material constitutive models [12]. Cracks are expressed by means of a multi-directional smeared fixed cracking approach [20] based on the active crack method. For RC structures constructed with normal-strength materials, several examples of validation have been reported, including [11]; however, there are few examples of validation for high-strength materials.

The study is based on two-dimensional FE analysis. When analyzing RC beams with a three-dimensional arrangement of reinforcement, such as when stirrups are present, a quasi-three dimensional analysis is implemented by superimposing two plate elements that share nodes in the depth direction. It has been confirmed that full three-dimensional analysis and this quasi-three dimensional approach produce almost identical results [21].

4.2 Analytical model for high-strength concrete

When analyzing members and structures containing high-strength concrete, simply applying the material constitutive equations for normal-strength materials as is would fail to adequately reflect their different properties. In high-strength concrete, aggregates particles split and the crack surface is smooth (**Photo 1**). For this reason, the amount of stress transferred along crack planes is lower. This cannot be expressed by merely changing the strength value in the existing constitutive models for normal-strength materials. It is also important to incorporate information on differences in the crack surface. This study considers two issues that are peculiar to high-strength concrete: tension softening of plain concrete after cracking and the reduction of stress transfer along crack planes. Since this study focuses on shear failure prior to yielding of main reinforcement, concrete compression and steel stress of main reinforcing bars should not in general exceed strength. Thus, there is no consideration of compression softening of high-strength concrete and plasticity of high-strength steel, and the conventional models are used.

Photo 1 Crack surface of high-strength concrete

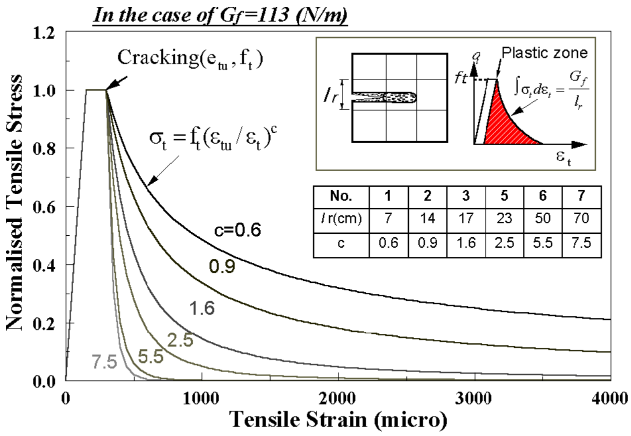

Fig. 15 Identification of tension release rate [21][27]

In the analysis model used in this study [21], the tensile stress release rate for each plain concrete element is determined such that consistency of the tensile fracture energy is satisfied in accordance with Eqs. (3) and (4), as shown in **Fig. 15**.

$$\int_{\varepsilon_{tu}}^{\varepsilon_{te}} \sigma_c(\varepsilon_c)d\varepsilon_c + \frac{1}{4} f_t \varepsilon_{tu} = G_f / l \tag{3}$$

$$\sigma_c = f_t \left(\varepsilon_{tu} \big/ \varepsilon_c \right)^C \text{; after cracking} \tag{4}$$

where, G_f is fracture energy (N/mm), l is element size (mm), ε_{tu} is cracking strain, ε_{te} is ultimate tensile strain, and C is stress release rate.

The authors have in the past used the CEB-FIP Model Code equation [22] described in Eq. (5) to calculate fracture energy. However, it seems inappropriate to apply this equation to high-strength concrete. Accordingly, for this study, we expand the scope of the model to include high-strength concrete and use Eq. (6) proposed by Uchida et al [23]; this has been verified by cement, fine aggregate, and coarse aggregate manufacturers throughout Japan. The CEB-FIP equation provides even larger fracture energy at high concrete compressive strengths than the latter equation.

$$G_f = \alpha_f \left(f_c' / 10 \right)^{0.7}, \quad \alpha_f = 1.25 d_{\max} + 10 \text{; (CEB)} \tag{5}$$

$$G_f = \alpha_f f_c'^{1/3}, \quad \alpha_f = 10 d_{\max}^{1/3} \text{; (Uchida et al.)} \tag{6}$$

where, G_f is fracture energy (N/m) and d_{max} is maximum aggregate size (mm).

The authors adopt a contact density function model [24] that has been proposed as a constitutive equation for stress transfer along the crack plane. When the strength of the mortar matrix is lower than that of the aggregate, the shape of the crack surface is independent of compressive strength and a single geometric shape can be assumed. Accordingly, the contact density function expressing the surface can be fixed and only stiffness at the contact point is then expressed as a function of compressive strength. In the case of high-strength concrete, however, the coarse aggregate splits when cracking occurs, so the crack surface is smooth and the stress transfer mechanism changes. By setting an appropriate contact density function corresponding to the shape of the crack surface, it is possible to express stress transfer behavior along crack surface of high-strength concrete. According to Bujadham et al, for a compressive strength range of approximately 60-100 MPa, it has been confirmed that stress transfer drops to around 20-50 % of that in the normal-strength concrete model, although this value does vary with crack opening width, as shown in **Fig. 16** [13][25]. This value is predicated on the condition that no meandering of cracks takes place; it is thought that it would be somewhat larger in an actual structure, but this has not yet been confirmed.

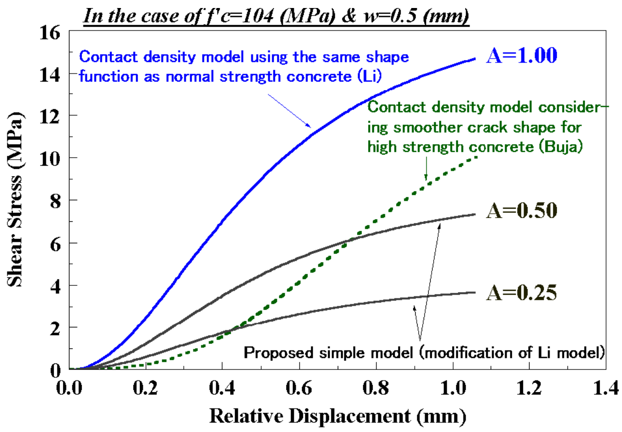

Fig. 16 Shear transfer model [13][24]

When applying numerical analysis to actual structures and members constructed with high-strength concrete, the complicated universal shear transfer constitutive equation proposed by Bujadham, for which stiffness at the contact point is not uniform, is suitable for joints, etc. as a discrete crack model. However, although this equation is rigorous, it is not currently practical to apply it to RC and plain concrete elements based on the smeared crack model. Here, the stress transfer equation is simplified by multiplying the shear transfer envelope (Eq. (7)) of the contact density function model [24] that assumes the rough crack surface of normal-strength concrete by a reduction coefficient A (< 1.00). (**Fig. 16**) As values of this shear transfer reduction coefficient important when considering structural behavior, A = 0.25 has reasonable applicability to the universal shear transfer constitutive equation in cracking width domains of 0.1 mm or less, A = 1.00 is the same as the normal-strength concrete model, and A = 0.50 is the middle value. These values will be studied and discussed later.

$$\tau = A\tau_{normal} = Af_{st}\frac{\beta^2}{1+\beta^2} \tag{7}$$

where, τ is shear stress transferred along crack plane, A is shear transfer reduction coefficient ($A \leq 1.00$ in the case of high-strength concrete), τ_{normal} is basic shear stress transferred along the crack surface, f_{st} is ultimate shear transfer strength ($= 3.83{f'_c}^{1/3}$), and β is the ratio of shear slip and opening displacement on the crack surface.

The shear behavior of cracked concrete can be calculated by combining the stress transfer model for crack planes, as expressed in Eq. (7), with the concrete stiffness between cracks [20]. In addition, compressive stress in the normal direction accompanying contact with the crack surface is calculated by uniformly multiplying the basic equation by the shear transfer reduction coefficient A. For high-strength concrete, this is a means of dealing with the reduction in compressive stress, in the same manner as shear stress.

In the case of self-compacting concrete, it has been reported that superb local bond may be obtained as non-breezing phenomenon can be expected around reinforcing bars, [26]. Bond properties are expressed as tension stiffening in the RC domain. The tension stiffening of self-compacting concrete has not yet been determined. However, analysis indicates good agreement between load (shear force) and deflection, as shown later, in which the effect of the tension stiffening model is significant. Accordingly, in this study, the existing model [12] is applied as is to the high-strength domain; the format of the equation is not changed at all and the cylinder strength of concrete is simply substituted.

5. APPLICATION OF TWO-DIMENSIONAL FINITE ELEMENT ANALYSIS

5.1 Test Series 1

Analytical results for Specimens 1-9 are shown along with the experimental results in **Figs. 2-1** through **2-9**. The analytical mesh is shown in **Fig. 17**; the domain 80 mm from the bottom of the beam for Specimens 1-4 and 9 (which each have a single row of main reinforcement) or 100 mm for Specimens 5-8 (which have double row of main reinforcement) is treated as the RC domain where bond action of the main reinforcement is apparent [27]. Calculations are terminated when the average shear strain within a finite element increases suddenly and reaches 1 %. This moment represents the point where loading exceeds the maximum capacity and the response behavior has reached the softening range. Here, uni-axial tensile strength of concrete in each specimen is determined from the flexural cracking load by means of backward estimation. The values used are 2.35 MPa for specimens with high-strength concrete and 1.76 MPa for specimens with normal-strength concrete. Both of these values are lower than the material test results obtained from splitting tests on circular pillar test pieces. In reality, however, it is reported that due to the effects of drying/autogenous shrinkage and the like, the actual strength of concrete in structural members would be lower [31].

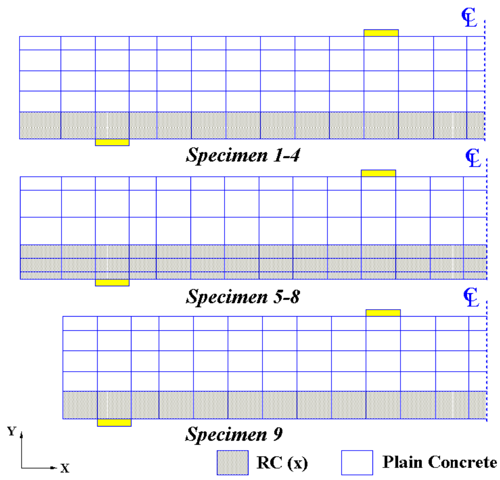

Fig. 17 Series 1 analytical mesh

In Specimens 2, 4, 6, and 8 constructed with normal-strength concrete, diagonal cracking occurs regardless of main reinforcement strength and can be evaluated comparatively well up until softening (**Figs. 2-2**, **2-4**, **2-6**, and **2-8**). These results are in line with previous studies [20]. However, the subsequent increase in load-carrying capacity after diagonal cracking, as seen in specimens with double row of main reinforcement, is not seen. This is true also for the high-strength concrete specimens to be discussed later.

Parametric analysis is carried out for high-strength concrete Specimens 1, 3, 5, 7 and 9, with the shear transfer reduction coefficient A set at 1.00, 0.50, and 0.25 (**Figs. 2-1**, **2-3**, **2-5**, **2-7** and **2-9**). According to the research by Bujadham et al., the average shear transfer reduction coefficient was approximately 0.25. The phenomenon of crack opening and shear slip initiating in the plain concrete element directly above an RC element and leading to failure is seen in all analysis cases. **Figs. 18-1** through **18-6** show the crack pattern derived from analysis of Specimens 1 and 5, which are constructed with both high-strength concrete and high-strength reinforcement. When the upper row of reinforcement in each diagram reaches maximum capacity in the analysis, the lower row is at the softening stage, and the specimens exhibit crack opening strain on the left side and shear strain along the crack surface on the right side. The deformation is illustrated with a magnification of 10 times for clarity (in these and subsequent figures).

As the shear transfer reduction coefficient is reduced from 1.00 to 0.50 and then 0.25, the following trends become evident:
(1) The propagation of secondary cracking that is not perpendicular to the initially introduced cracks is reduced;
(2) The critical cracking angle at which the shear strain radically increases approaches the vertical direction (perpendicular to the member's axis);
(3) The domain within which damage is concentrated tends to consist of plain elements around the bottom of the loading point at the center.
(These trends are conspicuous if the bottom diagrams in Fig. 18-1 and in Fig. 18-3.) Here, secondary cracking refers to the phenomenon in which the cracking progresses from flexural cracking to diagonal cracking as a result of the comparatively coarse elements.

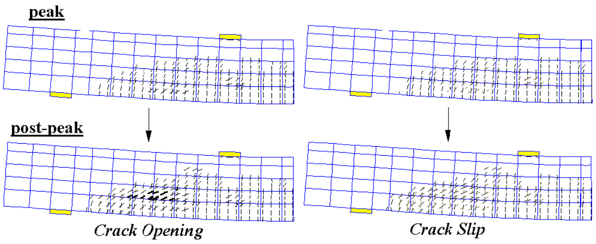

Fig. 18-1 No.1 crack pattern (A=1.00)

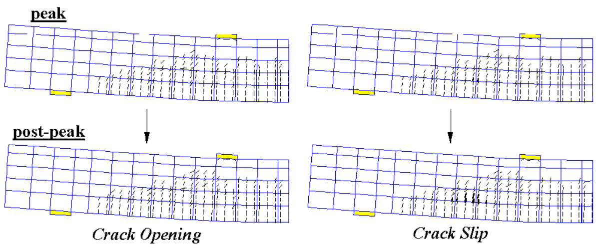

Fig. 18-2 No.1 crack pattern (A=0.50)

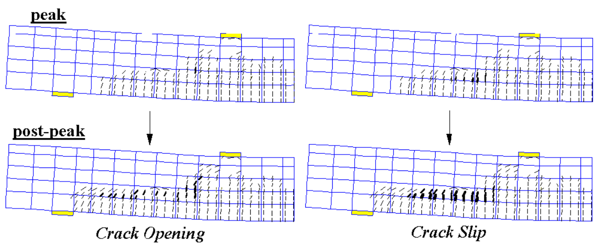

Fig. 18-3 No.1 crack pattern (A=0.25)

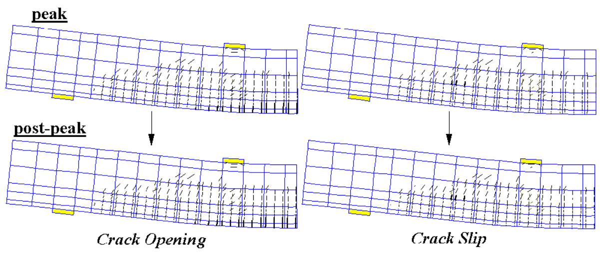

Fig. 18-4 No.5 crack pattern (A=1.00)

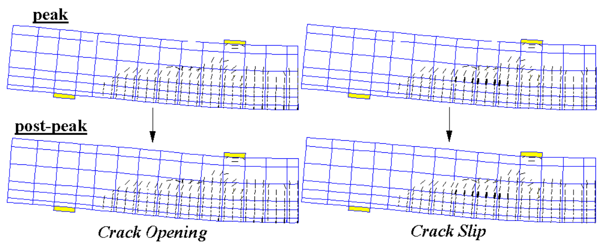

Fig. 18-5 No.5 crack pattern (A=0.50)

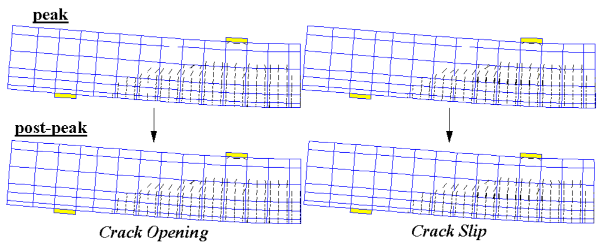

Fig. 18-6 No.5 crack pattern (A=0.25)

Judging from the above relationship between shear force and deflection and the cracking distribution, it is determined that a shear transfer reduction coefficient of 0.50 generally results in good correlation with the experimental results. In a previous study [12], a shear transfer verification test using mortar (with which the cracked surface is smooth, as with high-strength concrete) with a uniform crack width was of 0.5 mm gave almost the same results. In this test, it was found that the experimental and theoretical results matched closely when a shear transfer reduction coefficient of 0.40 was used.

The splitting of coarse aggregate along the crack surface may be physically treated as equivalent to mortar with a maximum aggregate diameter of 5 mm or less. The figure of 5 mm corresponds to the maximum diameter of the fine aggregate. Furthermore, when the shear transfer reduction coefficient is set to 0.50, diagonal cracking capacity increases gradually compared to the increase of concrete strength in the analysis as well (**Figs. 2-1** through **2-9**).

With Specimens 5 and 7, with a double row arrangement of main reinforcement, shear capacity decreases as the shear transfer reduction coefficient is reduced. However, with Specimens 1 and 3, which have a single row of main reinforcement, shear capacity changes with shear transfer reduction coefficient in the following order: 0.50 > 1.00 > 0.25. Based on these results, further consideration of the failure mechanism and beam capacity follows.

As noted above, reducing the shear transfer reduction coefficient has a dual effect. First, it obstructs the propagation of secondary cracking, and secondly it reduces the shear force supported by the cracked surface. With Specimen 1, which has a single row of main reinforcement, when the shear transfer reduction coefficient is 1.00, secondary cracking in the diagonal direction first occurs in RC elements along the main reinforcement, and this crack progresses through the web; ultimately, the crack width and shear strain increase in plain concrete elements and the ultimate state is reached. Conversely, when the shear transfer reduction coefficient is 0.50 and 0.25, the form of the fracture is different, with propagation of the secondary crack being reduced. In other words, the progress of diagonal cracking is obstructed. Damage is conspicuous in plain concrete elements, with shear strain increasing along the crack surface at almost a 90-degree angle. Softening behavior then appears. Due to these contrary actions, when the shear transfer reduction coefficient is 1.00 and 0.50, the maximum capacity is reversed. This demonstrates that shear transfer along the crack surface plays very important role in the domain in which flexural cracking changes to diagonal cracking.

With Specimen 5, which is provided with a double row arrangement of main reinforcement, even when the shear transfer reduction coefficient is 1.00, almost no secondary cracking in the diagonal direction occurs, and the result is primarily the extension of flexural cracking into diagonal cracking. The effect of differences in reinforcement arrangement and changes in effective depth is clearly seen in the analysis. Primary cracking associated with major deformation is almost completely perpendicular to the member axis. When the shear transfer reduction coefficient is 0.50 and 0.25, the localized regions of deformation are concentrated at the bottom of plain concrete elements near the loading points, and failure takes almost the same form as when the shear transfer reduction coefficient is 1.00. The obstruction of secondary cracking seen with Specimen 1 is not observed at all. For this reason, it is supposed that the shear transfer reduction coefficient and the maximum capacity are almost directly proportional. In the experiments, the diagonal crack that progressed from flexural cracking in the region near the loading points of Specimen 5 did not lead immediately to failure; rather, secondary and tertiary diagonal cracking took place at even smaller angles, leading to the ultimate state (**Photo 2**). The analysis is thought to have successfully modeled the progress up to the development of initial diagonal cracking.

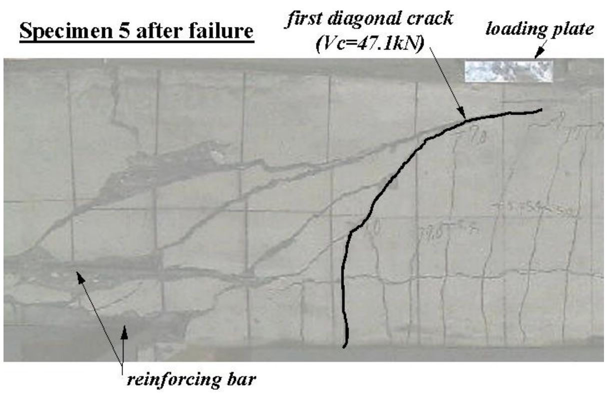

Photo 2 Specimen 5 crack distribution (enlarged)

Next, with the objective of conducting a more intensive study of the effects of fracture energy and shear transfer, comparative sensitivity analysis is implemented for Specimens 1 and 5. A comparison of the fracture energy values derived with Eqs. (5) and (6) shows that they are 136.0 N/mm and 111.6 N/mm, respectively, for a compressive strength of 69.5 MPa. Analysis is conducted under identical conditions for the two specimens, apart from calculation of the stress release rate of plain concrete elements from the fracture energy. **Figs. 19-1** and **19-2** show the analytical results based on CEB-FIP Eq. (5). The fracture energy is higher as compared with analytical results using the Uchida Eq. (6) (shown in **Figs. 2-1** and **2-5**), so the shear capacity is greater. This trend is particularly notable in the case of Specimen 5 with the double row arrangement of main reinforcement. The change in capacity resulting from varying the shear transfer reduction coefficient is similar in both cases. When analyzing RC beams constructed with high-strength concrete, it is important to consider not only the fracture energy but also shear transfer.

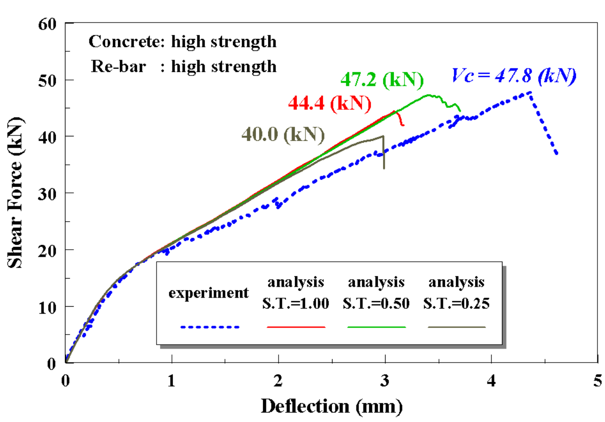

Fig. 19-1 No.1 parametric analysis of fracture energy

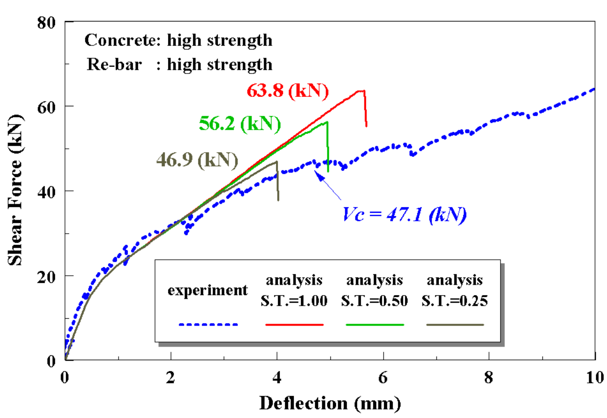

Fig. 19-2 No.5 parametric analysis of fracture energy

In the analysis described above, the same shear transfer reduction coefficient is applied to the zone in which there is a bond effect of main reinforcement (the RC zone) and the zone in which this is not present (the plain concrete zone). Now, different shear transfer reduction coefficients are applied to these two zones to confirm their effect using sensitivity analysis. The subjects of the analysis are Specimens 1 and 5. Making the most of numerical analysis, in which material properties are easily changed to hypothetical values in order to observe response behavior, sensitivity analysis is implemented for six cases of shear transfer reduction coefficient pairings for the RC zone and the plain concrete zone: (1.00, 0.25), (0.50, 0.25), (0.25, 0.25), (1.00, 1.00), (0.50, 1.00) and (0.25, 1.00). The fracture energy is calculated in accordance with Eq. (6). The analytical results are shown in **Figs. 20-1** and **20-2**.

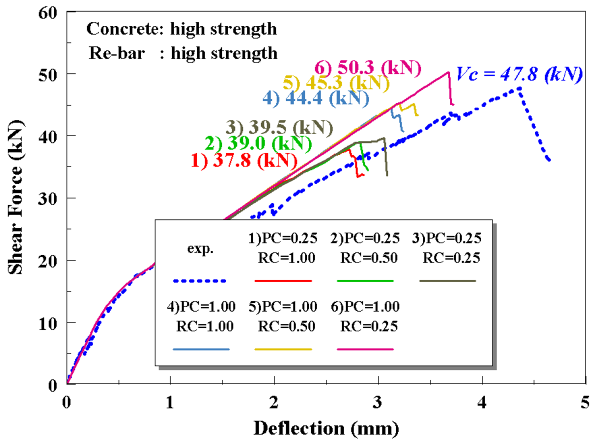

Fig. 20-1 No.1 parametric analysis of shear transfer

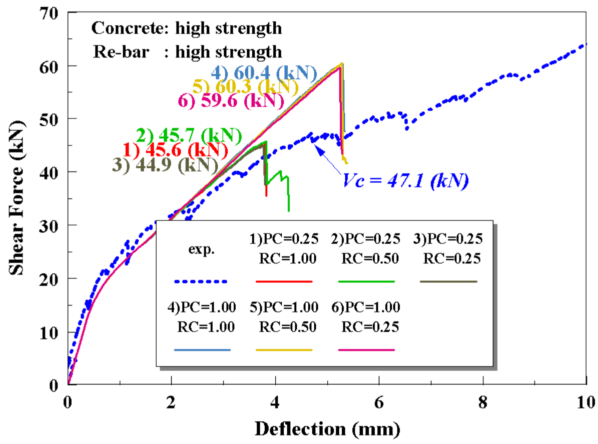

Fig. 20-2 No.5 parametric analysis of shear transfer

For Specimen 1 with a single row of main reinforcement, the greatest influence on shear capacity is the shear transfer reduction coefficient for plain concrete elements; the greater the coefficient is, the greater the capacity becomes (**Fig. 20-1**). The shear transfer reduction coefficient for RC elements also has an effect on calculated capacity, but in a comparison made by keeping the reduction coefficient for plain concrete elements constant, it is found that the lower the reduction coefficient for RC element is, the greater the capacity becomes. In the sensitivity analysis, the combination of shear transfer reduction coefficients that yields the highest capacity is 0.25 and 1.00, respectively, for RC and plain concrete elements.

In the case of Specimen 5, with a double row arrangement of main reinforcement, it is found that the shear transfer reduction coefficient for plain concrete elements has the greatest influence on shear capacity. The larger this coefficient is, the greater the capacity becomes. In this respect, the results are the same as for Specimen1 (**Fig. 20-2**). However, for RC elements, the shear transfer reduction coefficient has almost no effect on capacity. When the shear transfer reduction coefficient for RC elements is set to 0.25, the capacity merely drops somewhat.

These results of comparative analysis back up the interpretation made after calculations with the shear transfer reduction coefficient set to a constant value for both RC and plain concrete elements.

They show indirectly that the transferred shear stress of high-strength concrete reduces even in structural members. In the shear transfer test conducted for a single crack formed by creating a linear slit, the reduction was 0.25. In contrast, in the sensitivity analysis performed for cracking in an actual structure, a value of 0.50 gives good results. This difference may reflect the degree of meandering in the cracks produced in the structure, but at this point it is impossible to say for certain what the cause is; this is an issue that requires future study. In subsequent analysis and studies, the discussion is developed with the shear transfer reduction coefficient provisionally set to 0.50.

5.2 Test Series 2

Figs. 5-1 and **5-2** show the experimental results together with the analytical results. The analytical mesh is shown in **Fig. 21**. The area 37.5 mm from the bottom of the beam edge is assumed to be the RC domain in which bond action of the main tensile reinforcement is present (the RC zone). In order to take into account the three-dimensional arrangement of reinforcing bars in two-dimensional analysis, the section at a web height of 175 mm is defined using overlap elements. The overlap elements are designed to reflect the effect of the side reinforcement, which is to disperse diagonal cracks, and they consist of an RC element extending 75 mm and a plain concrete element extending 175 mm in the depth direction. A comparative analysis is also conducted for Specimen N250 with RC elements for the entire depth. In each analysis, when the average shear strain increases suddenly in an element where fracturing is concentrated and capacity softening appears, it is judged that shear failure occurs and calculation is terminated. The uni-axial tensile strength of each specimen is derived through backward estimation from the actual flexural cracking load. In specimens fabricated with normal-strength materials, its value is 1.72 MPa, while in specimens fabricated with high-strength materials it is 2.00 MPa.

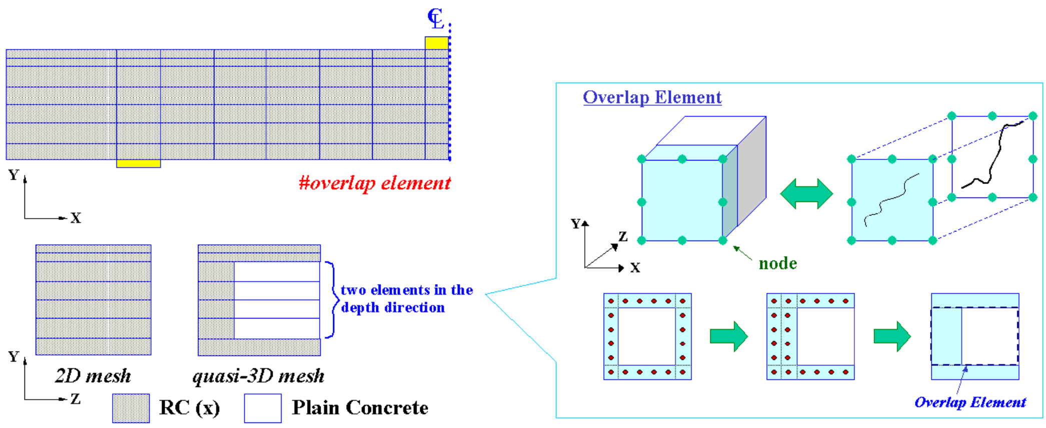

Fig. 21 Series 2 analytical mesh [29]

In the analysis of Specimen N250, whose reinforcement in the web depth direction is assumed to be uniformly distributed, shear failure occurs when, after flexural yield, the response displacement reaches approximately 4 δ_y. However, in the quasi three-dimensional analysis taking into account the local arrangement of reinforcing bars at the web, shear failure occurs before flexural yield as in actuality. A look at the cracking distribution shown in **Fig. 22** also indicates a clear difference, in terms of both angle and density, between cracking pattern in RC elements representative of the member surface and those inside the member (the plain concrete domain). This indicates that the mechanism of resistance to external stress is three-dimensional. In members where there is a localized arrangement of reinforcing bars, the effect of this three-dimensional mechanism must be taken into account. Some consideration of the three-dimensional effect, even if only by means of a quasi three-dimensional method, would enable it to be evaluated analytically. To improve accuracy, the method used to define domains for RC and plain concrete elements should be modified, replacing the current simple method with a more advanced one [28].

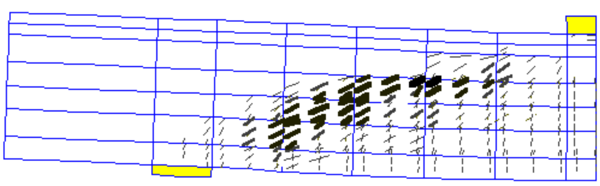

Fig. 22-1 N250 crack pattern (RC element)

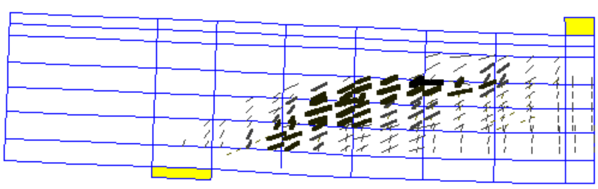

Fig. 22-2 N250 crack pattern (plain concrete element)

For Specimen H250, simulation is implemented with the shear transfer reduction coefficient set to 1.00 and 0.50. In the former case, the specimen reaches flexural yield and the ultimate state is reached at approximately 4 δ_y. In the latter, however, the value is slightly lower than the experimental value, but in general the capacity is properly evaluated. The fact that deformation capacity is estimated on the low side is thought to be because shear capacity and flexural capacity are in proximity to one another.

5.3 Test Series 3

Figs. 8-1 through **8-3** show the analytical results for Specimens 1-3 together with the experimental results. The study is performed with the shear transfer reduction coefficient set to 1.00 and 0.50. The analytical mesh is shown in **Fig. 23**. For Specimen 1 (medium size), the area 180 mm from the bottom of the beam edge is assumed to be the RC zone, while for Specimens 2 and 3 (large), it is the area 200 mm from the bottom. For Specimen 3, which is provided with web reinforcement, the RC zone in the vertical direction is determined in accordance with a zoning method [27] as in the Series 2 loading tests, based on the critical reinforcement ratio proposed by An et al., in order to define the overlap elements. For the purpose of comparison, a two-dimensional analysis is also implemented in which the web reinforcement is arranged uniformly in the member thickness direction. In each of these analyses, shear failure is judged to occur when the average shear strain increases and the maximum capacity is determined, and calculation is terminated at this point. As in the Series 1 and Series 2 loading tests, uni-axial tensile strength is determined by means of backward estimation from the actual flexural cracking load. Tensile strengths of each specimen are identified as 2.09, 2.04 and 2.29 MPa, respectively.

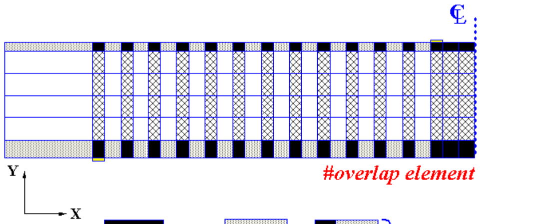

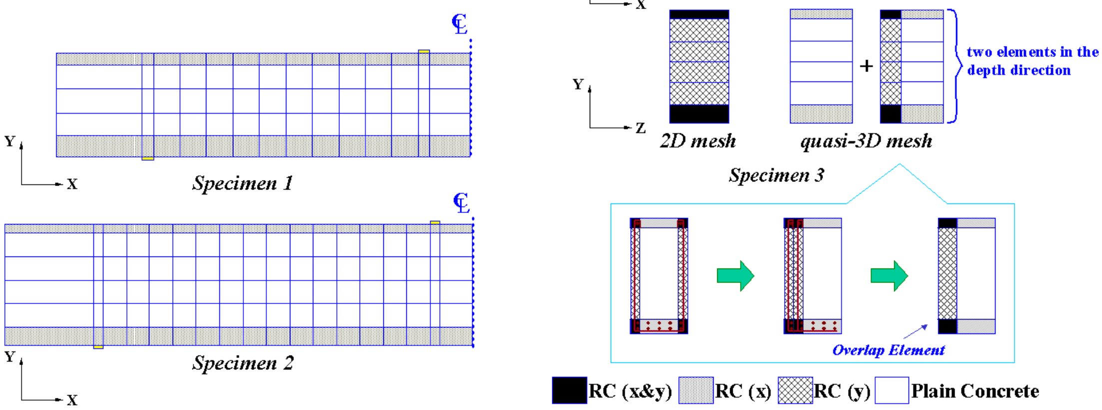

Fig.-23 Series 3 analytical mesh

With Specimens 1 and 2, which have no web reinforcement, the behavior up to initiation of diagonal cracking can generally be evaluated as in the Series 1 loading test (**Figs. 8-1** and **8-2**). This indicates that the size effect of shear capacity, which is interpreted as being more considerable than when normal-strength concrete is used, is calculated directly.

In the two-dimensional analysis of Specimen 3 (which has web reinforcement), where the three-dimensional arrangement of reinforcing bars is ignored, stable behavior is obtained after flexural yield. The shear strain increases, indicating the ultimate state, at around 5 δ_y when the shear transfer reduction coefficient is set to 1.00 and at about 4 δ_y when the shear transfer reduction coefficient is set to 0.50 (**Fig. 8-3**). A comparison of the ultimate cracking state, as shown in **Fig. 24-1**, reveals that when the coefficient is set to 1.00, the damage domain extends over a large area and the shear strain along the diagonal cracks is low; in contrast, when the coefficient is set to 0.50, the damage domain is narrower and the shear strain along the diagonal cracks is great.

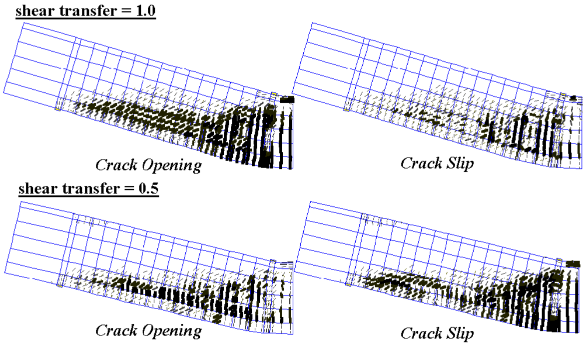

Fig. 24-1 Specimen 3 crack pattern (2D analysis)

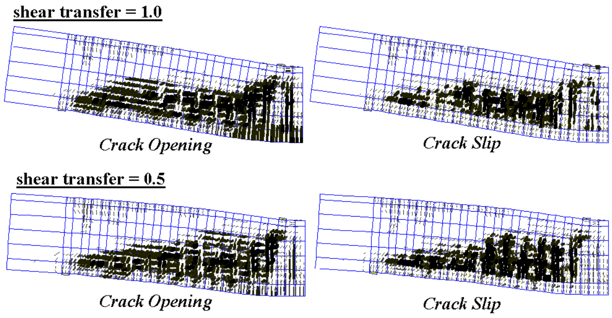

Fig. 24-2 Specimen 3 crack pattern (quasi-3D analysis)

Conversely, in the quasi three-dimensional analysis using overlap elements to take into consideration the localized arrangement of web reinforcement, when the shear transfer reduction coefficient is set to 1.00, shear failure occurs at about 2 δ_y. On the other hand, with the coefficient set to 0.50, even though the estimate of overall deformation is somewhat higher, as in the experiment, shear failure occurs almost simultaneously with flexural yield (**Fig. 8-3**). This demonstrates that consideration of the three-dimensional arrangement of web reinforcement can improve analytical accuracy of the shear behavior of RC beams. The fact that the increase in capacity after web reinforcement yield, which the modified Truss Theory is unable to explain, is automatically expressed in the analysis is worth noting. The adoption of a steel model [32] with improved precision through the localization of plasticity and rupture is thought to have led to these good analysis results.

The ultimate cracking state is characterized by the fact that damage is concentrated in the plain concrete elements. The fact that a reduction in the shear transfer mechanism leads to considerable shear strain along diagonal cracks can be seen as the same trend seen in specimens without web reinforcement (**Fig. 24-2**). However, by providing web reinforcement, the ultimate damage state changes to cover a comparatively wide area of the web without focus on the side of the loading points. This is quite consistent with the experimental results.

5.4 Test Series 4

Figs. 11-1 through **11-5** show the analytical results for Specimens 1-5 together with the experimental results. The shear transfer reduction coefficient is set to 1.00 and 0.50 in this study. The analytical mesh is shown in **Fig. 25**. The area 100 mm from the bottom of the beam edge is assumed to be the RC zone. The domain in which the web reinforcement has a bond effect is determined in the same manner as in the Series 3 loading tests. In each of the analysis cases, when the average shear strain increases and softening behavior is seen, it is judged that shear failure has occurred. The uni-axial tensile strength as determined through backward estimation is identified as 2.17, 1.70, 2.48, 1.87 and 2.17 MPa, respectively.

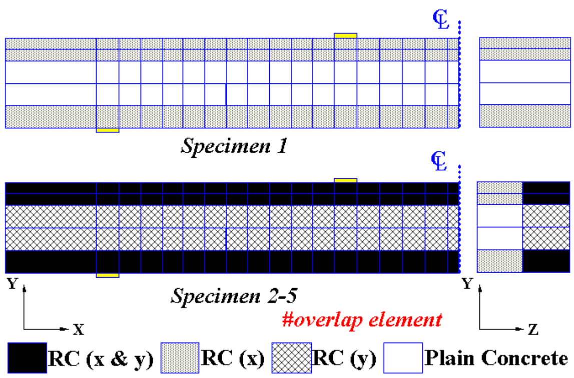

Fig. 25 Series 4 analytical mesh

With Specimen 1, which has no web reinforcement, the behavior up to diagonal cracking can generally be evaluated accurately, as is the case in the Series 1 and 3 loading tests. For Specimens 2-5, which have high-strength web reinforcement as well, shear failure can generally be evaluated up to softening using the same numerical approach as are used up to now (**Fig. 11**). The fact that capacity is slightly overestimated for

Specimen 5 is thought to derive from the discrete arrangement of web reinforcement at 200 mm intervals, which for analysis purposes is distributed uniformly in the member direction.

According to **Figs. 26-2** through **26-5**, which include the ultimate cracking state, only Specimen 4 of all beams with web reinforcement shows a tendency that diverges from the other specimens. This specimen has a combination of normal-strength concrete and high-strength web reinforcement. In this case, a decrease in capacity appears before diagonal cracking becomes widely distributed over the web section. In a comparison with experimental results and the modified Truss Theory equation using the actual yield strength value, V_{s_cal} is lower than V_{s_exp} in this specimen only. In the analysis, too, most of web reinforcement does not reach yield at the maximum capacity, and the strength of the steel with respect to the external force is not used effectively. The maximum average stress within elements of the lateral ties in Specimen 4 is 573 MPa in the ultimate state. With the other specimens, most of the lateral ties reach the yield stress and the average stress is widely distributed between 550 and 700 MPa.

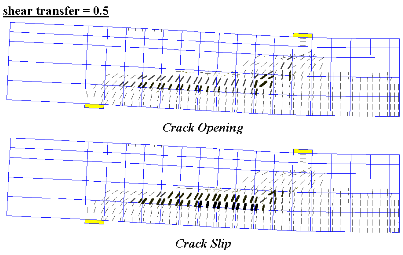

Fig. 26-1 No.1 crack pattern

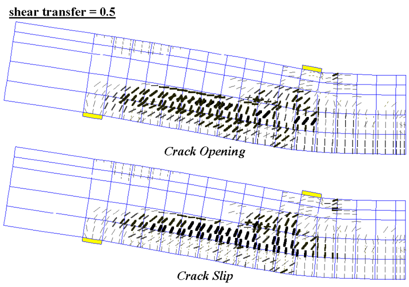

Fig. 26-2 No.2 crack pattern

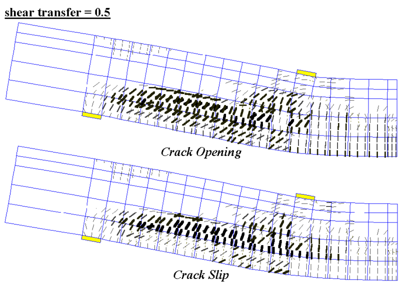

Fig. 26-3 No.3 crack pattern

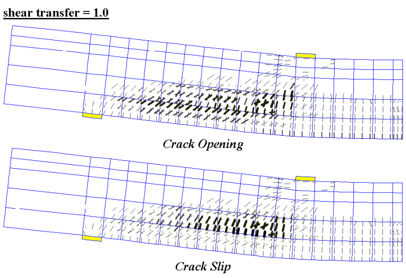

Fig. 26-4 No.4 crack pattern

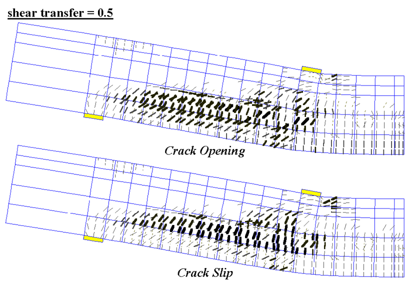

Fig. 26-5 No.5 crack pattern

From this study in which both experiment and theoretical analysis are carried out, it is confirmed that when using high-strength web reinforcement, it is necessary to consider not only the yield strength of the reinforcement but also concrete strength. In order to gain the maximum benefit from the use of high-strength reinforcement, it is deduced that efforts to prevent loss of concrete capacity are needed from the design stage. In future, a detailed study is required to look into the effects of both material properties and methods of reinforcing bar arrangement on the interaction between composite materials and failure mechanisms.

6. CONCLUSIONS

This study was an examination of the shear capacity of RC beam and column members made with self-compacting high-strength concrete and high-strength reinforcement, using both experiment and theoretical analysis. The conclusions drawn from the work are as follows:

1) As noted in previous studies, the diagonal cracking load in an RC beam member made with high-strength concrete peaks as concrete compressive strength increases. This seems to indicate the validity of the simple method used in the current design equation, in which an upper limit is placed on the strength term. However, when compared to normal-strength concrete, size effects tend to be more considerable. At the design stage, this should be taken into account along in the definition of safety factors.

2) A reinforcement effect equivalent to the yield strength is achieved when high-strength concrete is combined with normal-strength web reinforcement. The mechanism by which external force is resisted after diagonal cracking is thought to be the same as when normal-strength concrete is used, even though high-strength concrete exhibits a smooth crack surface.

3) When high-strength web reinforcement is used, simultaneous consideration of concrete strength offers the prospect of making full use of the yield strength of the reinforcing bars in design practice. If high-strength concrete is used, it may be possible to increase the design yield strength of the web reinforcement above the existing design value.

4) The authors focused on tension softening and shear transfer relating to smooth crack planes if high-strength concrete. A numerical analysis method for high-strength materials was proposed, and it was confirmed that the method is generally capable of evaluating the deformational behavior of RC beams. In addition to being accurate, this analysis method is shown to be simple and more direct than the current design equation.

Acknowledgements
The authors would like to express their gratitude to Professor Hajime OKAMURA and Dr. Masahiro OUCHI of Kochi University of Technology for the invaluable advice received during the course of this study.

References

[1] Okamura, H., Maekawa, K. and Ozawa, K., "High Performance Concrete", *Gihodo-Shuppan*, September 1993. (in Japanese)
[2] Social System Institution, "Self-Compacting High Performance Concrete –Record of Challenge from the Drawn into Application", edited by Okamura, H., March 1999. (in Japanese)
[3] S.Q.C. Structures Development and Popularization Association, *Proc. of the Symposium on Ultra High Performance Concrete Structures*, August 1998. (in Japanese)
[4] Masukawa, J., Amano, R., Suda, K. and Ohtsuka, K., "Development of RC High Pier Using High Strength Reinforcing Bars", *Concrete Research and Technology*, Vol.9, No.1 (issue 17), January 1998. (in Japanese)
[5] JSCE, "A Middle-Long Term Vision on the Revision of Standard Specification for Design and Construction of Concrete Structures –Report of Secretary Committee of Specification Committee, Concrete Committee-", *Concrete Technical Series 32*, September 1999. (in Japanese)
[6] Matsui, Y., Uchida, Y., Rokugoh, K. and Koyanagi, W., "Shear Capacity of Reinforced High-Strength Concrete Beams without Stirrups", *Proc. of JCI*, No.17, Vol.2, pp.655-660, 1995. (in Japanese)
[7] Abe, Y., Ito, K., Matsubara, K. and Suzuki, M., An Experimental Study on Shear Capacity of Reinforced Concrete Beams without Shear Reinforcement Using Ultra High Strength Materials", *Proc. of JCI*, Vol.21, No.3, pp.181-18, 1999. (in Japanese)
[8] Fujita, M. and Oodate, T., "Effect of Concrete Strength on Shear Fracture Yield Strength in Concrete Beam Members", *Proc. of JCI*, Vol.22, No.3, pp.955-960, 2000. (in Japanese)
[9] Shimono, K., Kashiwabara, S., Sato, T. and Matsuoka, S., "Experimental Study on Shear Strength Evaluation in Reinforced Concrete Beams Using High-Strength Materials", *Proc. of JCI*, Vol.21, No.3, pp.175-180, 1999. (in Japanese)
[10] JSCE, "Standard Specification for Design and Construction of Concrete Structures [Design]", 1996. (in Japanese)
[11] Maekawa, K., Tsuchiya, S. and Fukuura, N., "Nonlinear Analysis of Reinforced Concrete and Seismic Performance Evaluation", *Proc. of the Second Symposium on Nonlinear Numerical Analysis and its Application to Seismic Design of Steel Structures*, pp.1-16, JSCE, November 1998. (in Japanese)
[12] Okamura, H. and Maekawa, K., "Nonlinear Analysis and Constitutive Models of Reinforced Concrete", *Gihodo-Shuppan*, May 1991.
[13] Bujadham, B., Mishima, T. and Maekawa, K., "Verification of the Universal Stress Transfer Model",

Proc. of JACE, No.451/V-17, pp.289-300, August 1992.
[14] Niwa, J., Yamada, K., Yokozawa, K., and Okamura, H., "Reevaluation of the Equation for Shear Strength of RC Beams without Web Reinforcement", *Concrete Library of JSCE*, No.9, pp.65-84, 1987.
[15] Selby, R. G., Vecchio, F. J. and Collins, M. P., "Analysis of Reinforced Concrete Members Subjected to Shear and Axial Compression", *ACI structural journal*, Vol. 93, No. 3, May-June 1996.
[16] Tan, K., Kong, F., Teng, S. and Weng, L., "Effect of Web Reinforcement on High Strength Concrete Deep Beams", *ACI structural journal*, Vol. 94, No. 5, September-October 1997.
[17] Iguro, M., Shioya, T., Nojiri, Y. and Akiyama, H., "Experimental Studies on Shear Strength of Large Reinforced Concrete Beams under Uniformly Distributed Load", *Concrete Library of JSCE*, No.5, 1985.
[18] Haddadin, M. J., Hong, S.T. and Mattock, A.H., "Stirrup Effectiveness in Reinforced Concrete Beams with Axial Forces", *Journal of Structural Division, Proc. of ASCE*, September 1971.
[19] Okamura, H., "Limit State Design Method of Concrete Structure [Second Edition]", *Kyoritsu Shuppan*, May 1984. (in Japanese)
[20] Fukuura, N. and Maekawa, K., "Spatially Averaged Constitutive Law for RC In-Plane Elements with Non-Orthogonal Cracking as far as 4-Way Directions", *Proc. of JSCE*, No.634/V-45, pp.177-196, November 1999. (in Japanese)
[21] Hauke, B. and Maekawa, K., "Three-Dimensional Modelling of Reinforced Concrete with Multi-Directional Cracking", *Concrete Library International*, No. 36, pp.181-206, JSCE, December 2000.
[22] CEB Comite Euro-International du Beton, "CEB-FIP Model Code 1990".
[23] Nakamura, S., Kitsutaka, Y., Mihashi, H. and Uchida, Y., "Discussion on Standard Evaluation Method for Tension Softening Properties of Concrete", *Concrete Research and Technology*, JCI, Vol.1, No.1, pp.1151-164, 1991. (in Japanese)
[24] Li, B., Maekawa, K. and Okamura, H., "Contact Density Model for Stress Transfer across Cracks in Concrete", *Journal of the Faculty of Engineering, the University of Tokyo (B)*, Vol.XL, No.1, pp.9-52, 1989.
[25] Bujadham, B. and Maekawa, K., "The Universal Model for Stress Transfer across Cracks in Concrete", *Proc. of JSCE*, No.451/V-17, pp.277-287, August 1992.
[26] Yamamoto, H., Itoh, H., Mishima, T. and Shima, H., "Study on Properties of Steel Bar of Reinforced Concrete Structures Using High-Strength Material", *Proc. of JCI*, No.22, Vol.3, pp.1249-1254, 2000. (in Japanese)
[27] An, X., Maekawa, K. and Okamura, K., "Numerical Simulation of Size Effect in Shear Strength of RC Beams", *Concrete Library International*, No.31, pp.323-346, JSCE, June 1998.
[28] Niikura, I. And An, X., "Improvement of RC Zoning Model and Is Application to 3D FEM Analysis", *Proc. of JCI*, Vol.22, No.3, pp.169-174, 2000. (in Japanese)
[29] Tsuchiya, S., Nakahama, S. and Maekawa, K., "The Effect of Side Reinforcement on Shear Capacity of RC Beam and 3D Distribution of Diagonal Cracks", *Proc. of JCI*, Vol.23, No.3, pp.997-1002, 2001. (in Japanese)
[30] Yang, Y. Sato, R. and Xu, M., "An Experimental Study on Shrinkage and Its Restrained Stress of High Strength Concrete", *Proc. of JCI*, No.20, Vol.2, pp.631-636, 1998. (in Japanese)
[31] Vecchio, F. J. and Collins, M.P., "Response of Reinforced Concrete to In-Plane Shear and Normal Stresses", *University of Toronto*, Department of Civil Engineering Publication No.82-03, March 1982.
[32] Salem, H. and Maekawa, K., "Spatially Averaged Tensile Mechanics for Cracked Concrete and Reinforcement under Highly Inelastic Range", *Concrete Library International*, No.34, pp.151-169, JSCE, December 1999.
[33] Hara, N., Mishima, T., Yamada, N. and Kondo, M., "Shear Capacity of Reinforced Concrete Beams Using Self-Compacting High-Strength High-Durability Concrete", *Proc. of JCI*, No.23, Vol.3, pp.925-930, 2001. (in Japanese)